COO--3056-37

MASTER

There is no objection from the patent point of view to the [illegible] disclosure of [illegible] document(s) listed in this [illegible]

BROOKHAVEN PATENT GROUP

6/18 1979 By CRL

Thermo Electron CORPORATION

DISCLAIMER

Thermo Electron
CORPORATION

Report No. TE4258/4247-132-79

DOE/JPL ADVANCED THERMIONIC TECHNOLOGY PROGRAM

PROGRESS REPORT NO. 37

December 1978 - January 1979

DOE Contract EY-76-C-02-3056
JPL Contract 955009

Prepared by

Thermo Electron Corporation
101 First Avenue
Waltham, Massachusetts 02154

PART ONE: DOE TASKS

I. THERMIONIC CONVERTER PLASMA STUDIES

A. CONVERTER THEORY

In the original Thermo Electron plasma program,[1] it was assumed that the ion flow in the plasma is considerably less than the electron current. At the same time, the variation of ion current is equal to the absolute value of the variation of electron current. This results in a small relative variation of electron current across the plasma, even if there is intense ionization and a considerable variation of ion current. Therefore, electron current may generally be assumed to be constant across the plasma. Since the ion current density (J_i) is considerably less than the electron current density (J_e), it was further assumed that the electron current density equals the value of total current density (J) with negligible loss of accuracy; that is,

$$J = J_e + J_i \simeq J_e$$

If the charged particle density is in the order of 10^{13} cm^{-3} or less, the above assumption is valid. In the case of the charged particle density being in the order of 10^{14} cm^{-3} or higher, the above assumption may no longer be valid. For example, with an emitter temperature of 1600 K and a charged particle density of 10^{14} cm^{-3}, the ion current density at the plasma boundary is approximately 0.4 A/cm^2, which may have a significant effect on other parameters if the output current density is less than 10 A/cm^2. In order to evaluate the effect of ion current, the assumption that the electron current equals the total current through the plasma has been removed from the program. A comparison of observed and calculated J-V curves is shown in Figure 1 where the

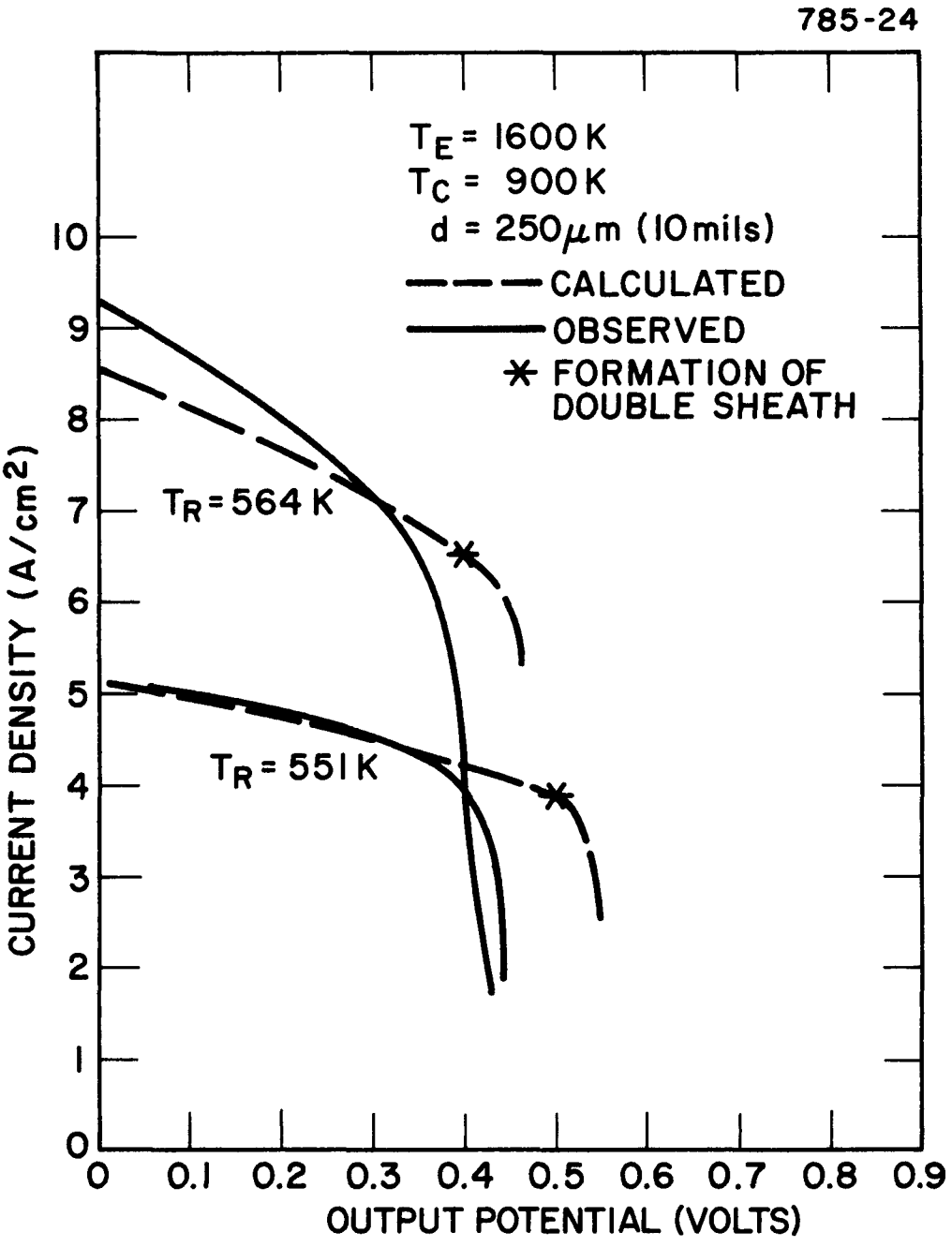

Figure 1. Comparison of Observed and Calculated J-V Curves for the Case T_E = 1600 K, T_C = 900 K, and d = 250 μm (10 mils) with $J_e = J_e^E$ = Constant

output current density is less than 10 A/cm^2, assuming that $J_e = J =$ constant. Figure 2 shows the same comparison, but with the assumption that $J = J_e(x) + J_i(x)$. In this case, the output potential at which the knee of the calculated characteristic appears is a good match to the measured value. These results demonstrate that calculations using the modified assumption are in better agreement with experiment than those using the assumption of constant electron current across the plasma.

II. LOW-TEMPERATURE CONVERTER DEVELOPMENT

A. CONVERTER NO. 209: TUNGSTEN EMITTER, LANTHANUM HEXABORIDE SHOWERHEAD COLLECTOR

This converter is equipped with a gas panel capable of admitting measured amounts of oxygen into the showerhead tubulation behind the collector. The converter has been outgassed and initial power data and collector work function data have been obtained.

Converter performance was measured at emitter temperatures of 1400, 1500, 1600 and 1700 K. Visual observation of the plasma showed a uniform discharge in the interelectrode space. Optimized cesium and collector performance curves at the four emitter temperatures are shown in Figures 3 through 6. Fully optimized curves at these temperatures are shown in Figure 7. The barrier index at 1400 K was 2.22 eV and increased to a value of 2.34 eV at 1700 K. Representative retarding plot and back emission data are shown in Figure 8. A barrier index of 2.22 eV at 1400 K is consistent with collector work function values (at appropriate T/T_R) measured by retarding plots. However, a rise in the barrier index at higher emitter temperatures is not indicated by collector work function measurements.

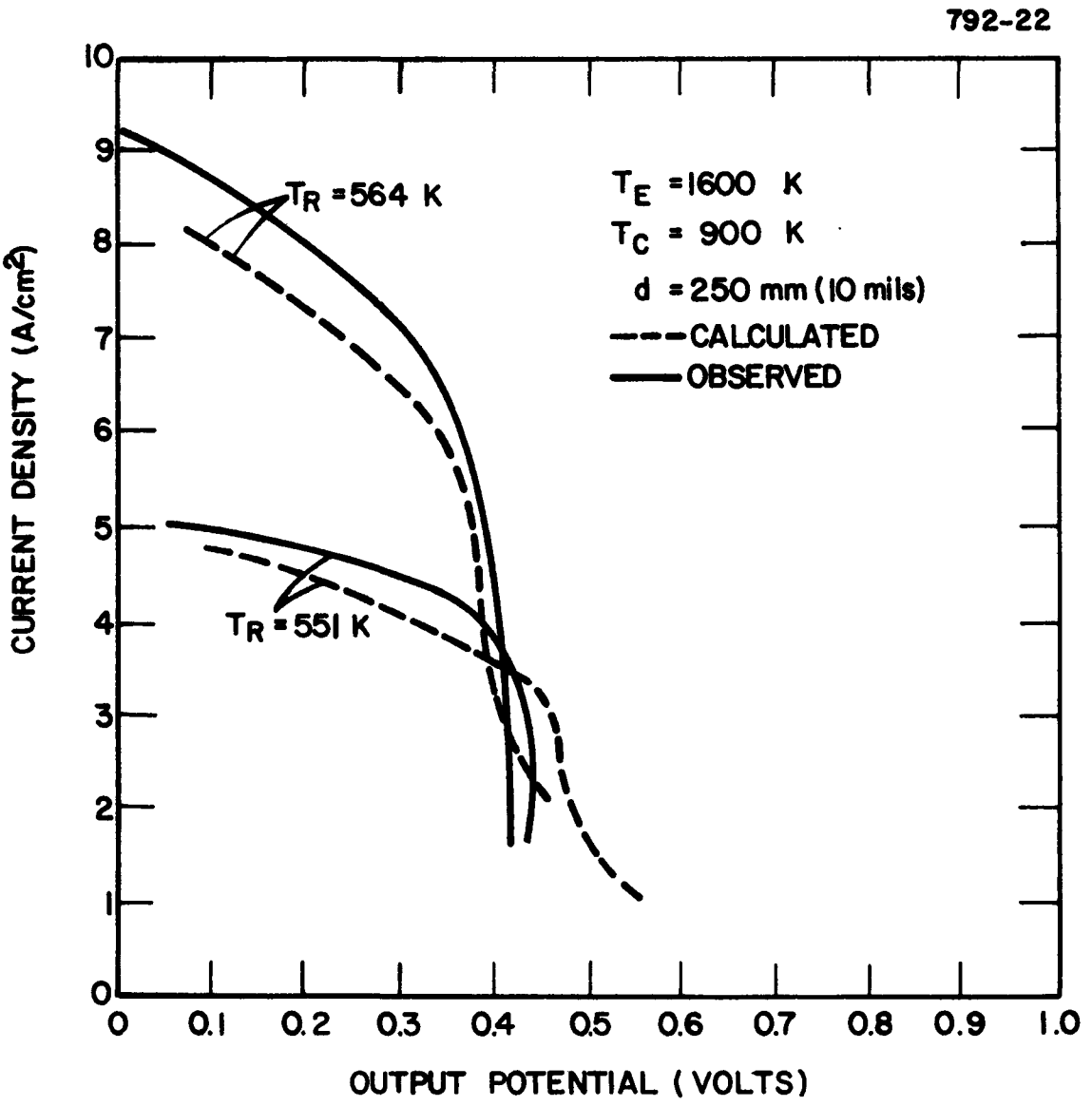

Figure 2. Comparison of Observed and Calculated J-V Curves for the Case T_E = 1600 K, T_C = 900 K, and d = 250 μm with $J = J_e(x) + J_i(x)$

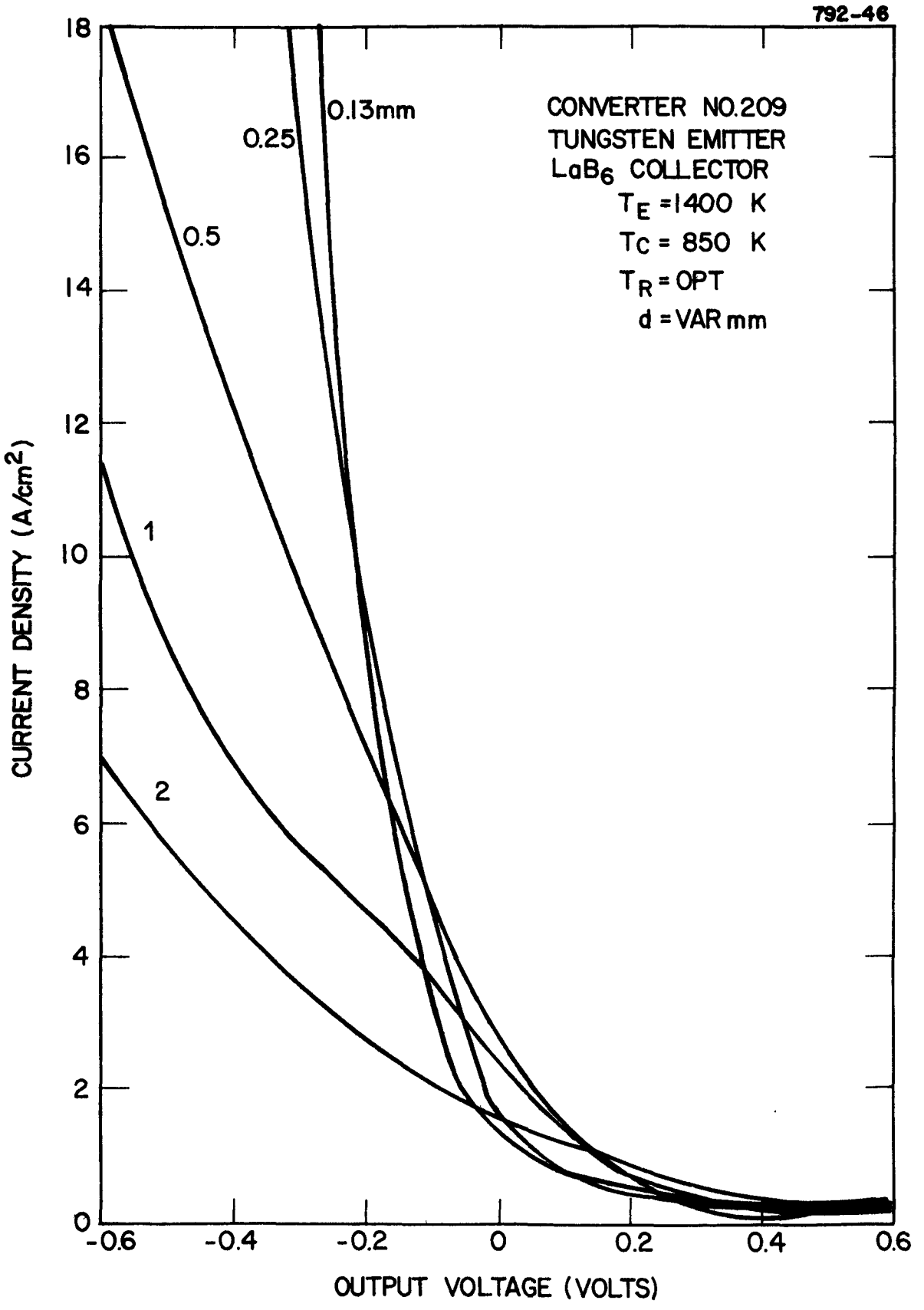

Figure 3. Cesium Optimized Converter Performance at Various Spacings, T_E = 1400 K

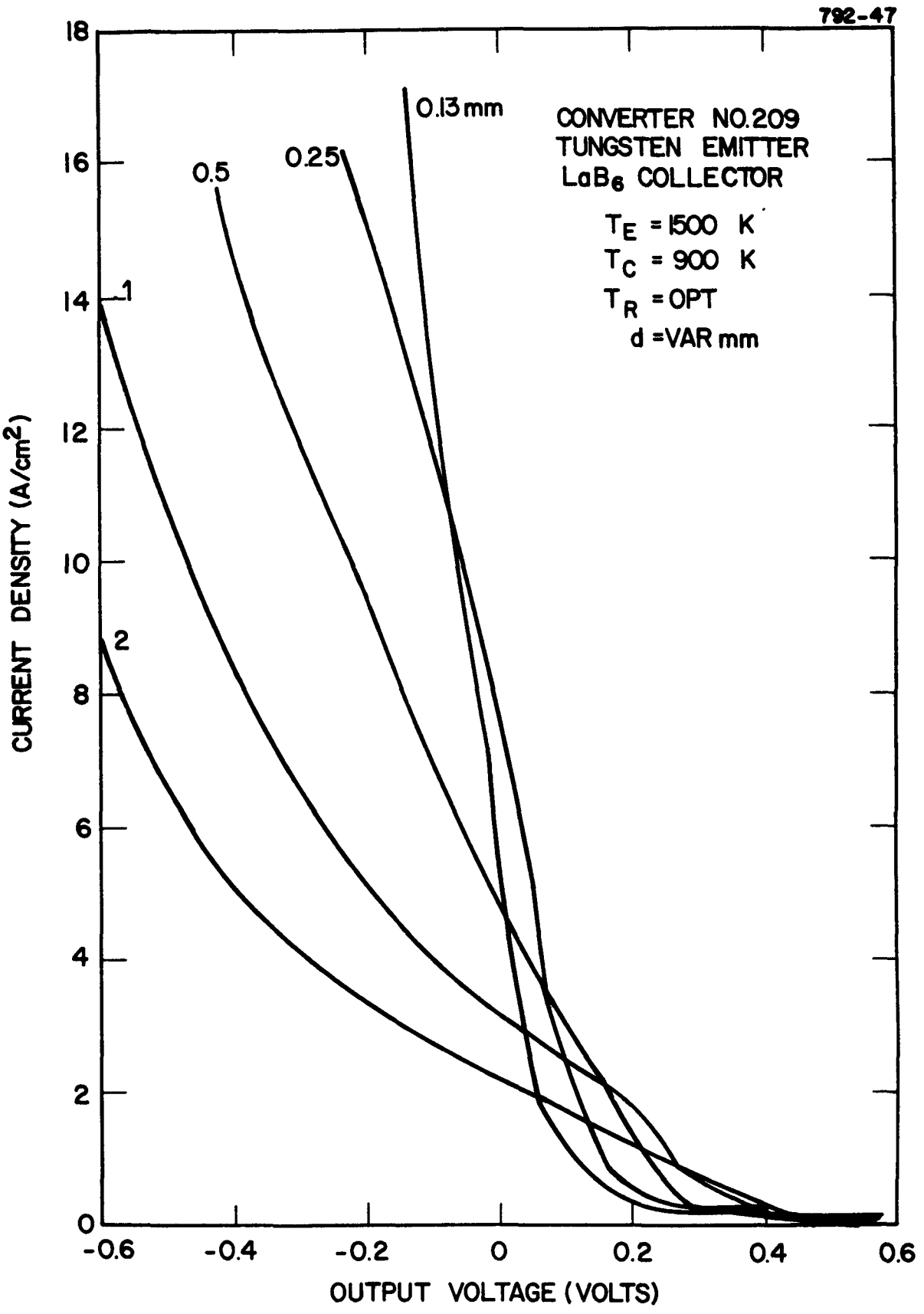

Figure 4. Cesium Optimized Converter Performance at Various Spacings, T_E = 1500 K

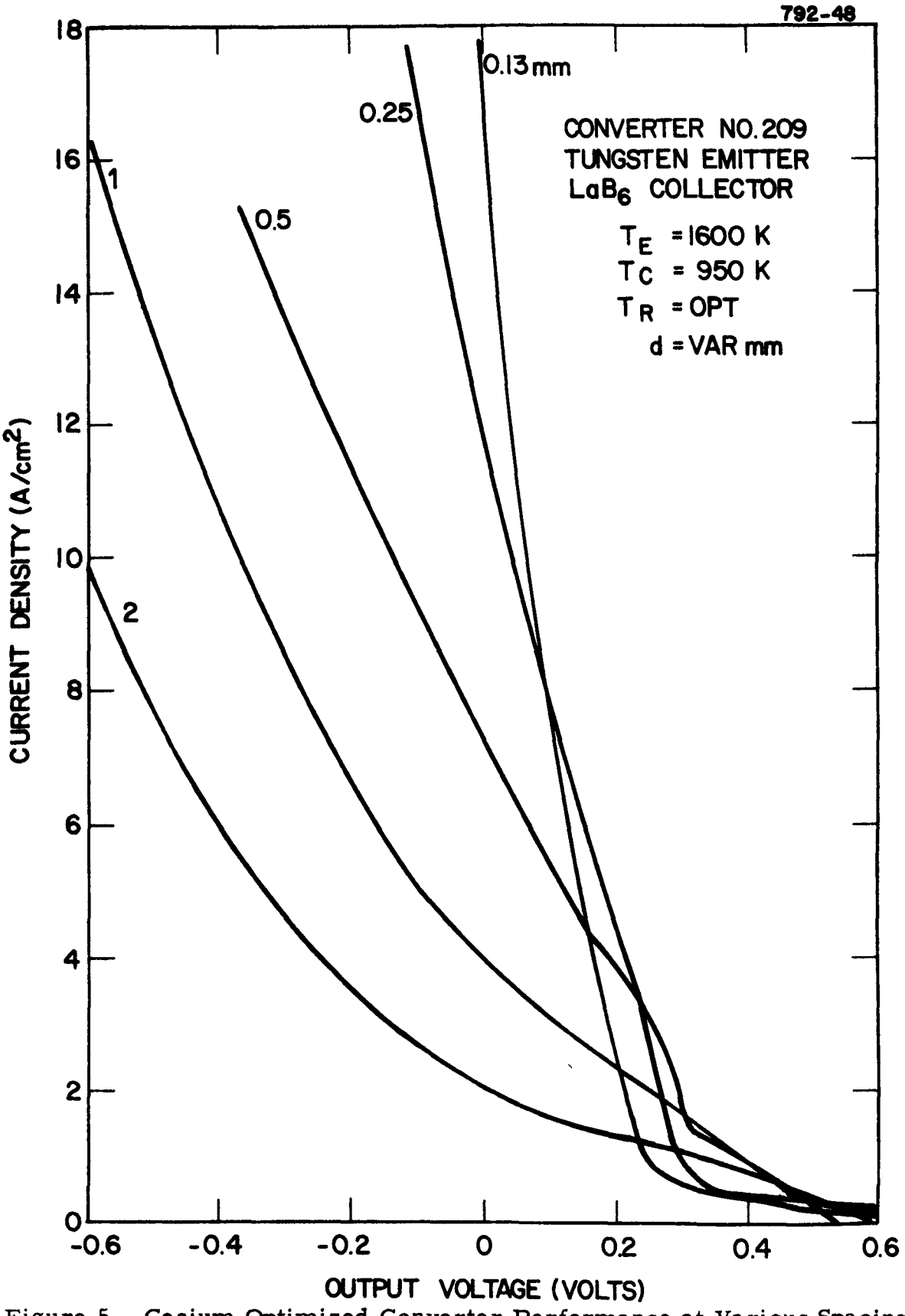

Figure 5. Cesium Optimized Converter Performance at Various Spacings, T_E = 1600 K

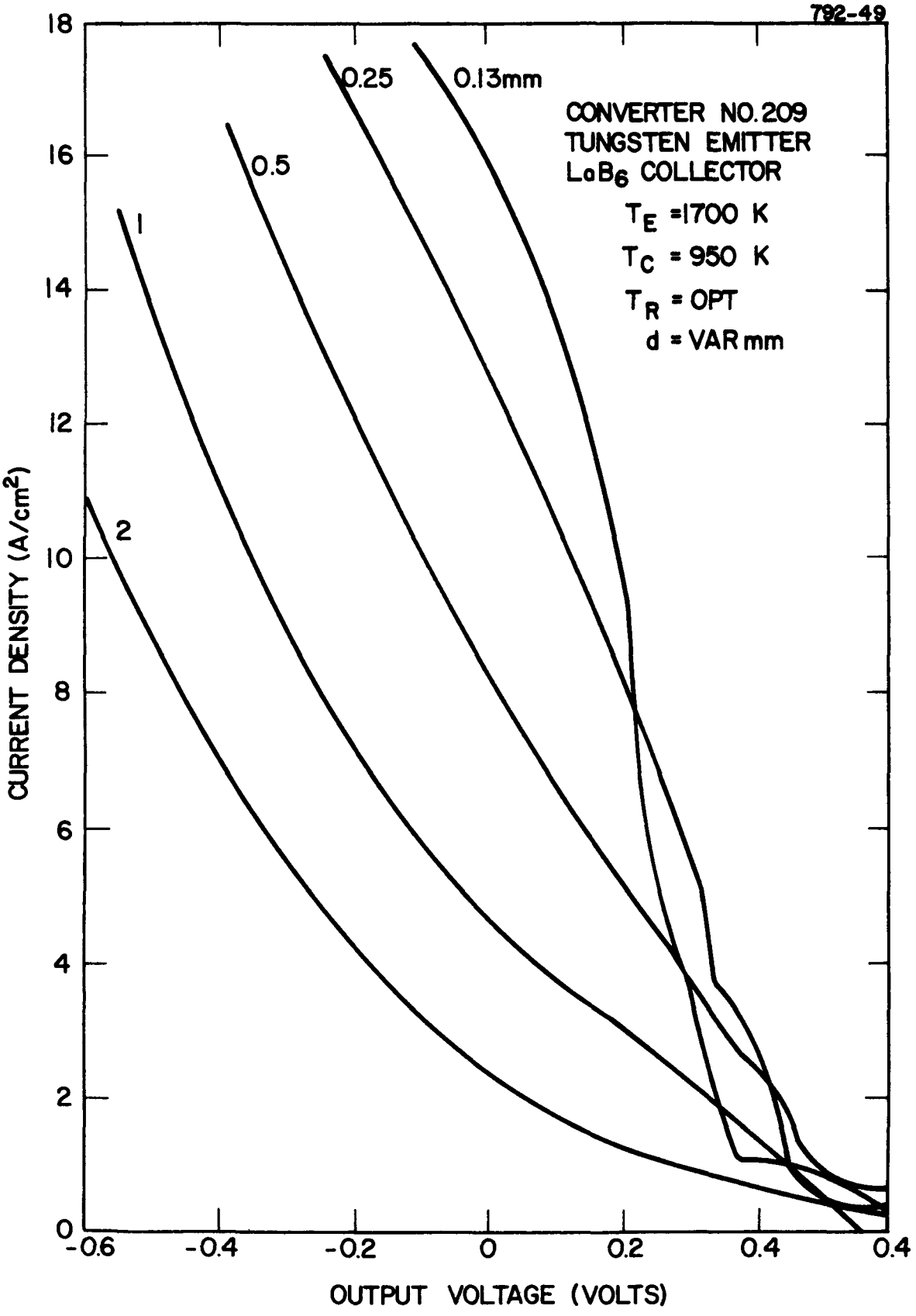

Figure 6. Cesium Optimized Converter Performance at Various Spacings, T_E = 1700 K

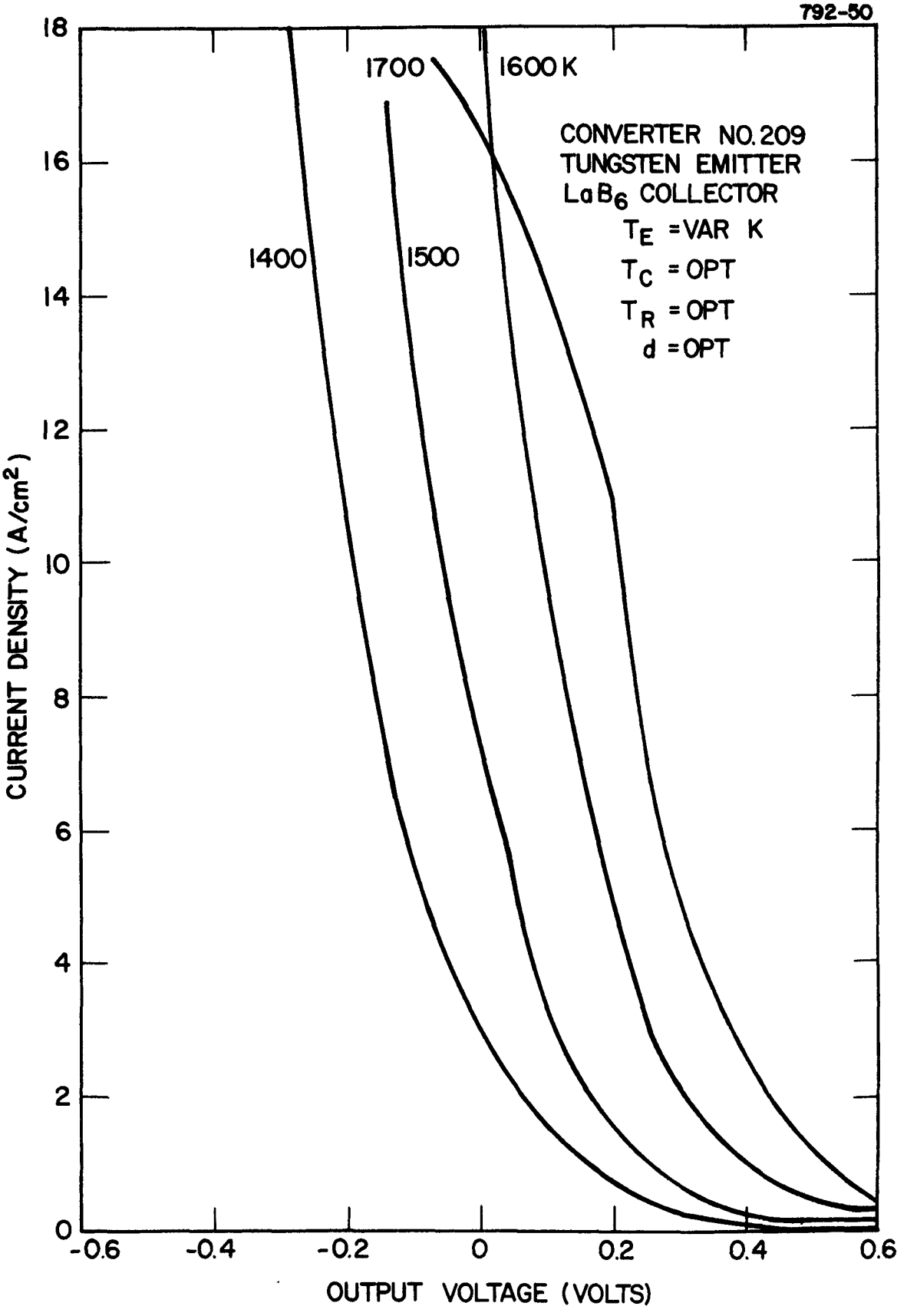

Figure 7. Fully Optimized Converter Performance at Several Emitter Temperatures

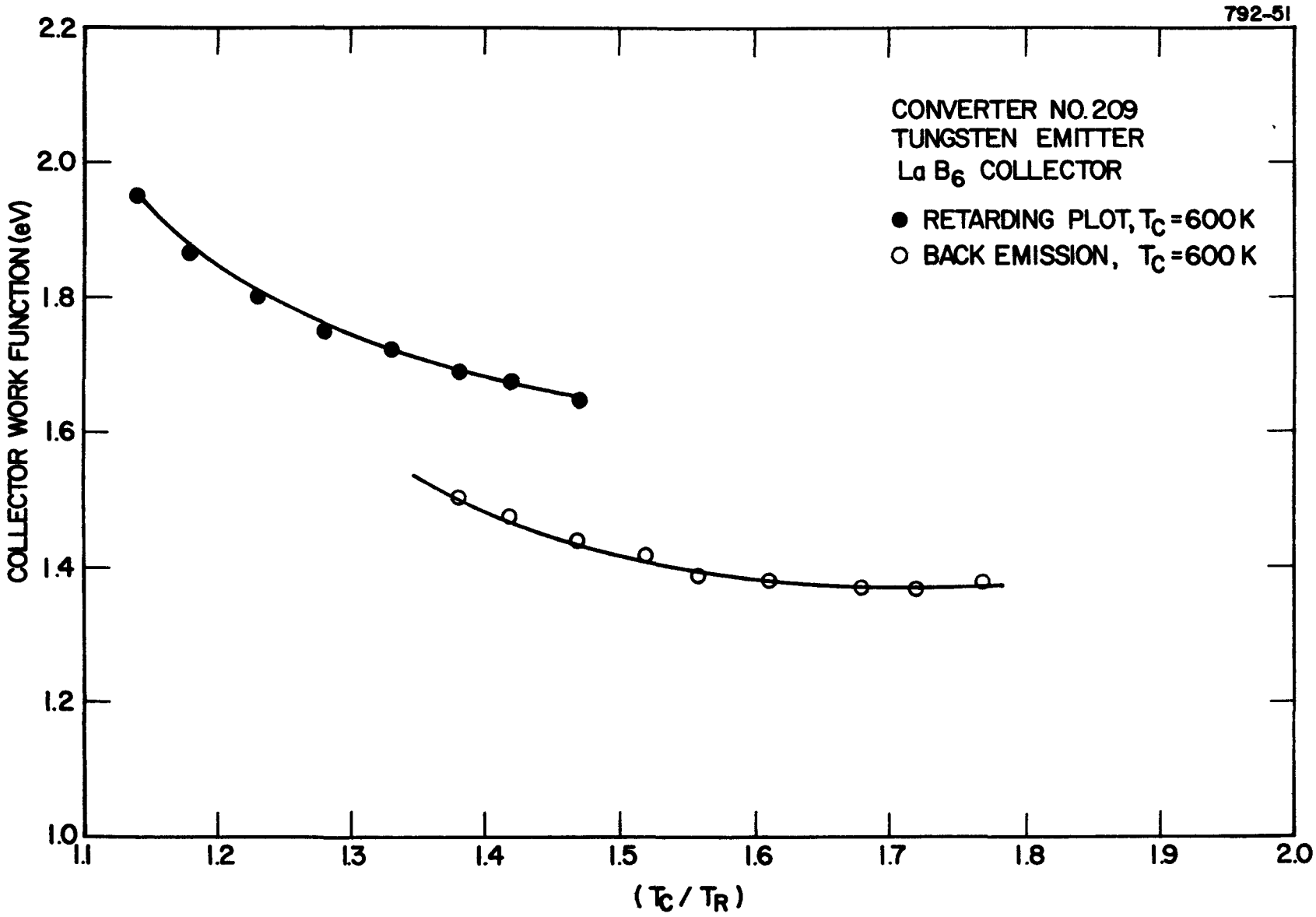

Figure 8. Collector Work Function versus the Ratio of Collector Temperature to Cesium Reservoir Temperature

Subsequent to completing the collection of power output data, measured amounts of oxygen will be introduced into the showerhead tubulation and the effects on converter performance measured.

B. CONVERTER NO. 207: TUNGSTEN EMITTER, TUNGSTEN OXIDE COLLECTOR

An attempt to activate this converter in the same manner as other tungsten oxide converters failed. After several hundred hours at collector and cesium reservoir temperatures of 700 and 551 K, respectively, a high series resistance was still apparent from the J-V characteristics. The collector temperature was then raised to 750 K to expedite the activation process. After operating at this temperature for approximately 900 hours, the collector seemed to become more conductive. At this time a barrier index of 2.10 eV at 6 A/cm^2 was measured at emitter, collector, and cesium reservoir temperatures of 1400, 750 and 487 K, respectively. The associated data are shown in Figure 9. The high emission at low cesium pressures indicates that the converter is well oxygenated. However, performance at an emitter temperature of 1750 K was not as good. A cesium family at T_E = 1750 K and T_C = 750 K is shown in Figure 10. Upon returning to T_E = 1400 K the performance shown in Figure 9 was not repeatable.

The minimum collector work function measured by the retarding potential method was 1.50 eV as compared to a 1.42-eV collector work function for the more successful Converter No. 206. The minimum work functions for both collectors occurred at the same T_C/T_R ratio

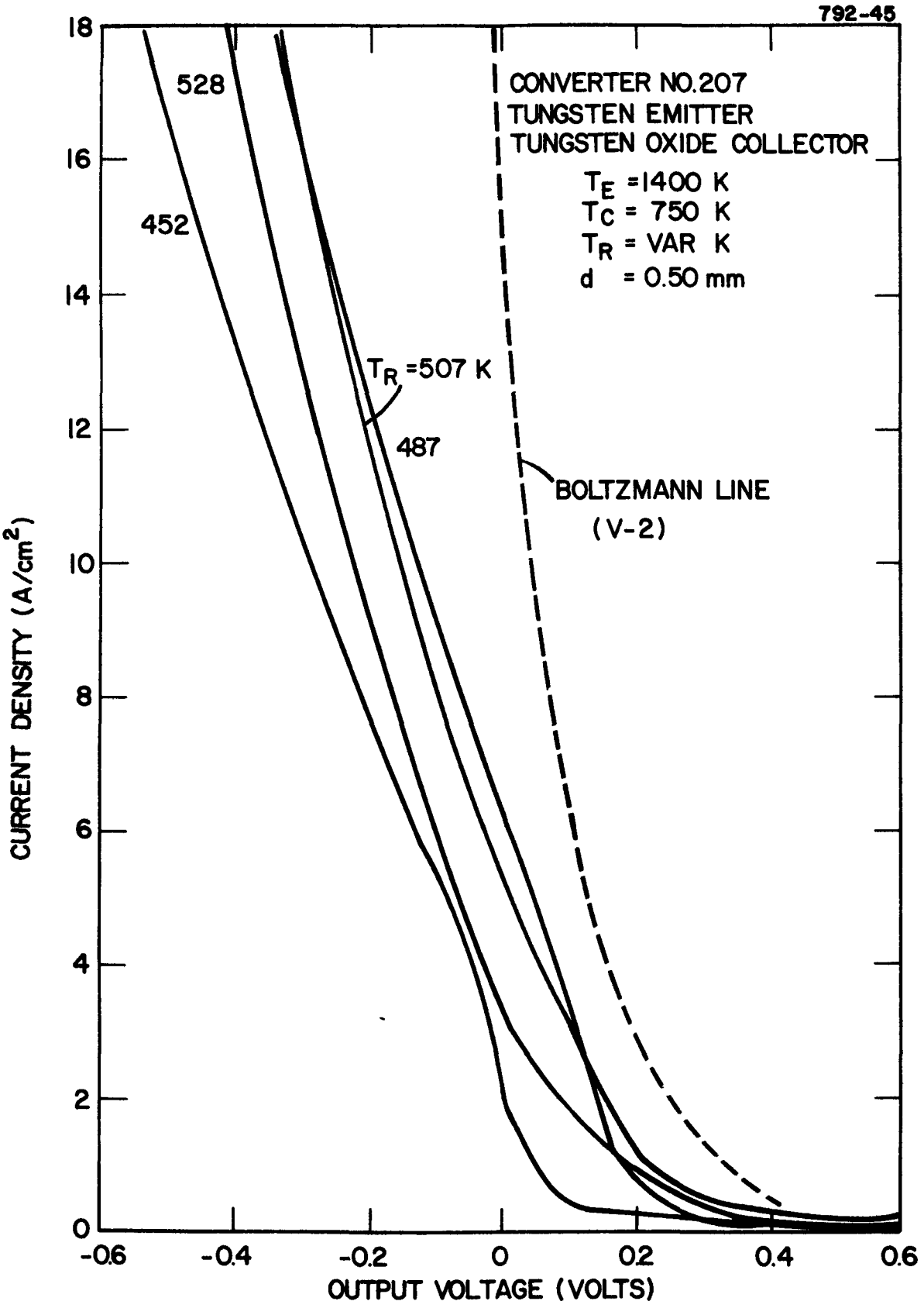

Figure 9. Cesium Family of Converter No. 207 at an Emitter Temperature of 1400 K

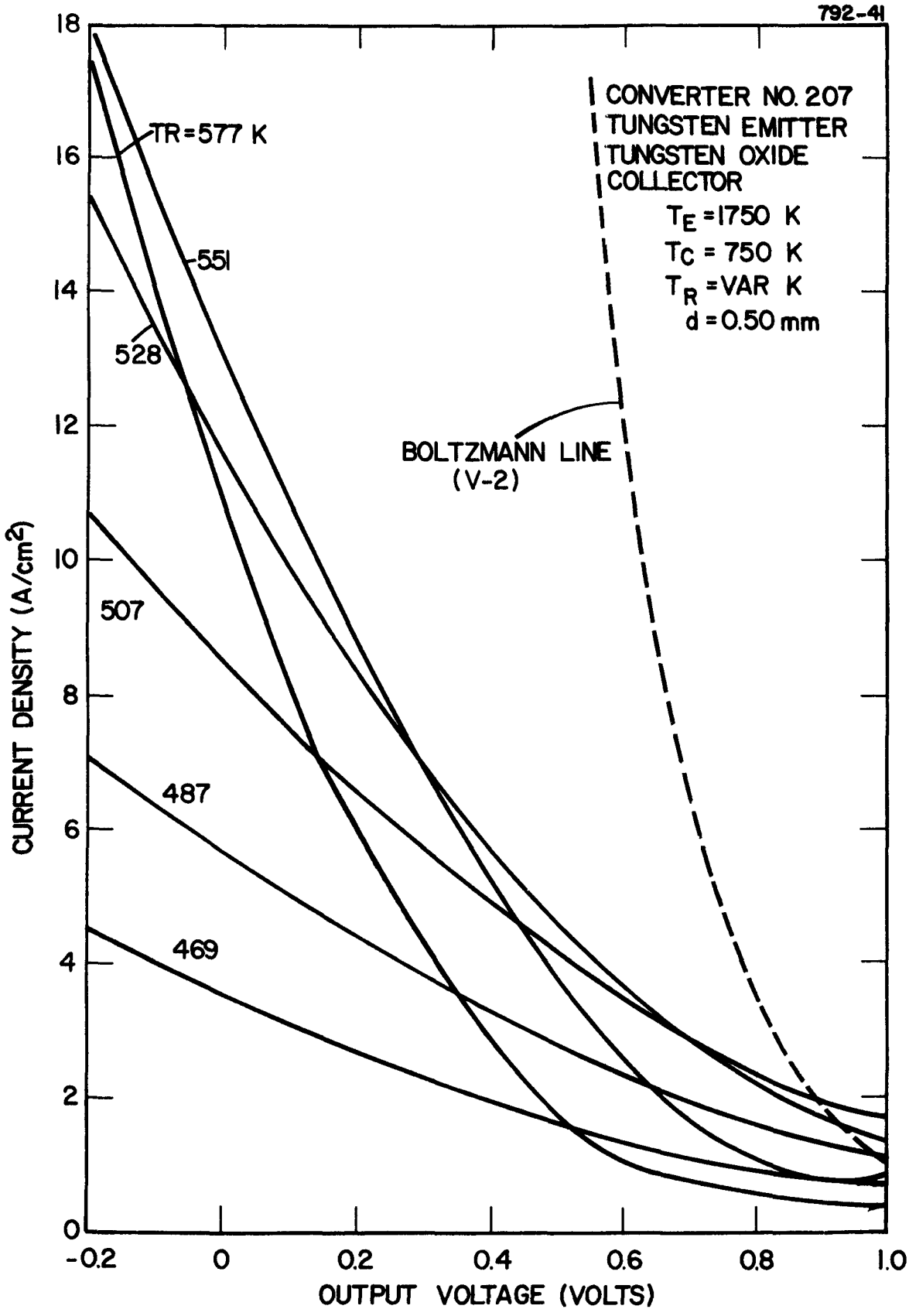

Figure 10. Cesium Family of Converter No. 207 at an Emitter Temperature of 1750 K

of 1.55. A plot of collector work function versus the ratio of collector temperature to cesium reservoir temperature is given in Figure 11. Attempts to improve the activation of this collector will continue.

C. PARTICLE CONVERTER EXPERIMENT

Work during this reporting period focused on the resolution of several problems associated with the building of a cesiated particle converter. A test device was constructed using a conventional variable-spacing test converter, except for the omission of the bellows assembly and the cesium reservoir. The emitter was molybdenum and the collector was a molybdenum cap brazed to a nickel substrate. The device was built and tested to answer the following questions:

a) Can the emitter and collector be uniformly sprayed with 1/2-mil thick coatings?

b) Can the variable-spacing apparatus of the test stand be used to bring the emitter and collector surfaces into contact after activation so that the surfaces will be sufficiently parallel?

c) After mating, will the activated coatings be electrically insulating?

After refinement of the existing spray technique, the emitter and collector surfaces were coated in their respective assemblies using the RCA composition of barium, strontium, and calcium oxides. Coating thicknesses on sample electrodes were determined to be approximately 1/2 mil.

A zero spacing reference was established by repeatedly shorting the bare electrodes and monitoring the micrometer reading. If proper care was taken in removing and replacing the electrode assemblies (for spraying), the zero reference was not changed significantly and the electrodes remained parallel.

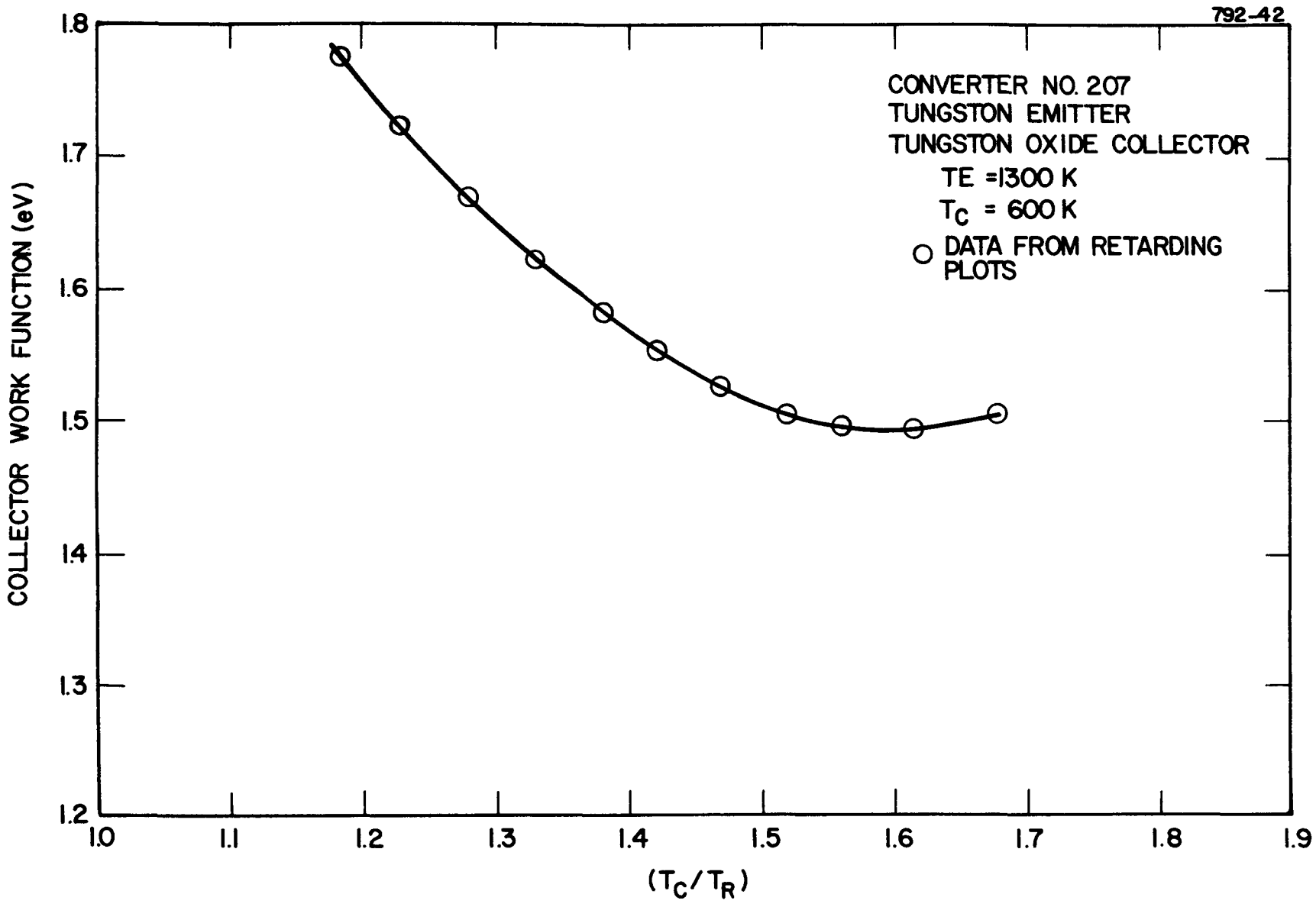

Figure 11. Retarding Plot of Collector Work Function versus the Ratio of Collector Temperature for Converter No. 207

The activation of the "barium oxide" coatings were incomplete because of exposure to the diffusion pump environment of the bell jar. After both electrodes were activated, the collector surface was lowered into contact with the emitter surface. No shorting was observed during subsequent testing although breakdown did occur when the potential across the electrodes exceeded one volt. Examination of the electrode surfaces after testing revealed resistive layers at the coating-substrate interfaces. Work has begun on the cesiated particle converter, utilizing the experience provided by the test device.

Tests on single electrodes coated with RCA "barium oxide" were also carried out in order to better understand the activation process. These tests were performed in a high-vacuum ion pump system.

III. COMPONENT HARDWARE DEVELOPMENT

A. CVD COMPONENT HARDWARE DEVELOPMENT

Eleven composite hot shells were fabricated during this reporting period. One graphite mandrel, 2 inches in diameter, was CVD coated with silicon carbide and was leak tight. Five of the 11 hot shells passed each of the leak tests and will be brazed to a molybdenum flange for flame testing.

Continuous efforts are concentrated on identifying leaks and determining exactly where each orginates on the composite hot shell. An initial leak test is made to confirm the absence of any leaks in the first deposit before the second deposit is made. This step is followed by two, and sometimes three, additional leak tests. Each test is more sensitive than the preceding one.

In the first leak test, the composite shell is mounted in a bell jar under vacuum for a minimum of 12 hours. It is then returned to atmospheric pressure with helium and soaked for 4 hours (see Figure 12A). The composite shell is then leak tested with a "sniffer" that detects any helium that might have been sorbed by the graphite via cracks in either the graphite or silicon carbide coating (see Figure 12B).

The more sensitive method has been to mount the helium-soaked composite shell in a bell jar connected to a helium leak detector (see Figure 12C). If any helium has been sorbed in the composite shell, it will be detected as it is pumped by the helium leak detector. The significant limitation to this method is its inability to locate the origin of the helium leaking from the composite shell.

A third test requires the removal of silicon carbide from the hemisphere of the composite shell to expose the graphite layer. The exposed graphite is coupled to a helium leak detector (see Figure 13) and helium is sprayed over the shell. If a leak exists, helium will pass through the opening in the graphite and register on the leak detector.

Only two shells have been tested in this destructive manner. The first had a leak located by the "sniffer" at the open end. The second had no leak revealed by the "sniffer" method, but one was detected by the bell jar method. As expected, the first shell continued to leak at the open end, but no leak could be found in the second shell. This contradicts the helium soak method. A possible explanation is that the graphite layer may be leaktight to the atmosphere and yet the interface of silicon carbide and tungsten may sorb helium during the soak

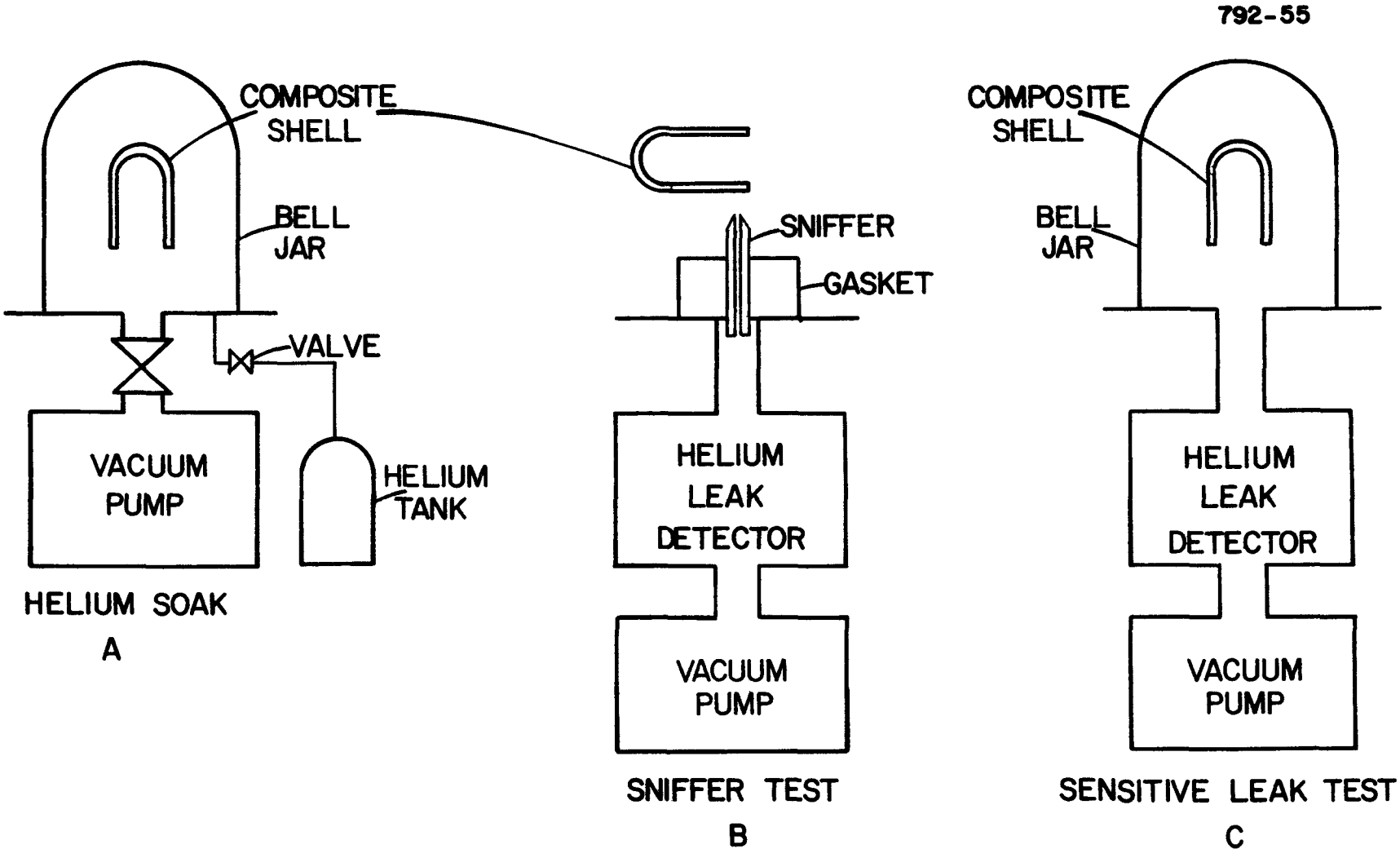

Figure 12. Composite Hot Shell Leak Test Methods

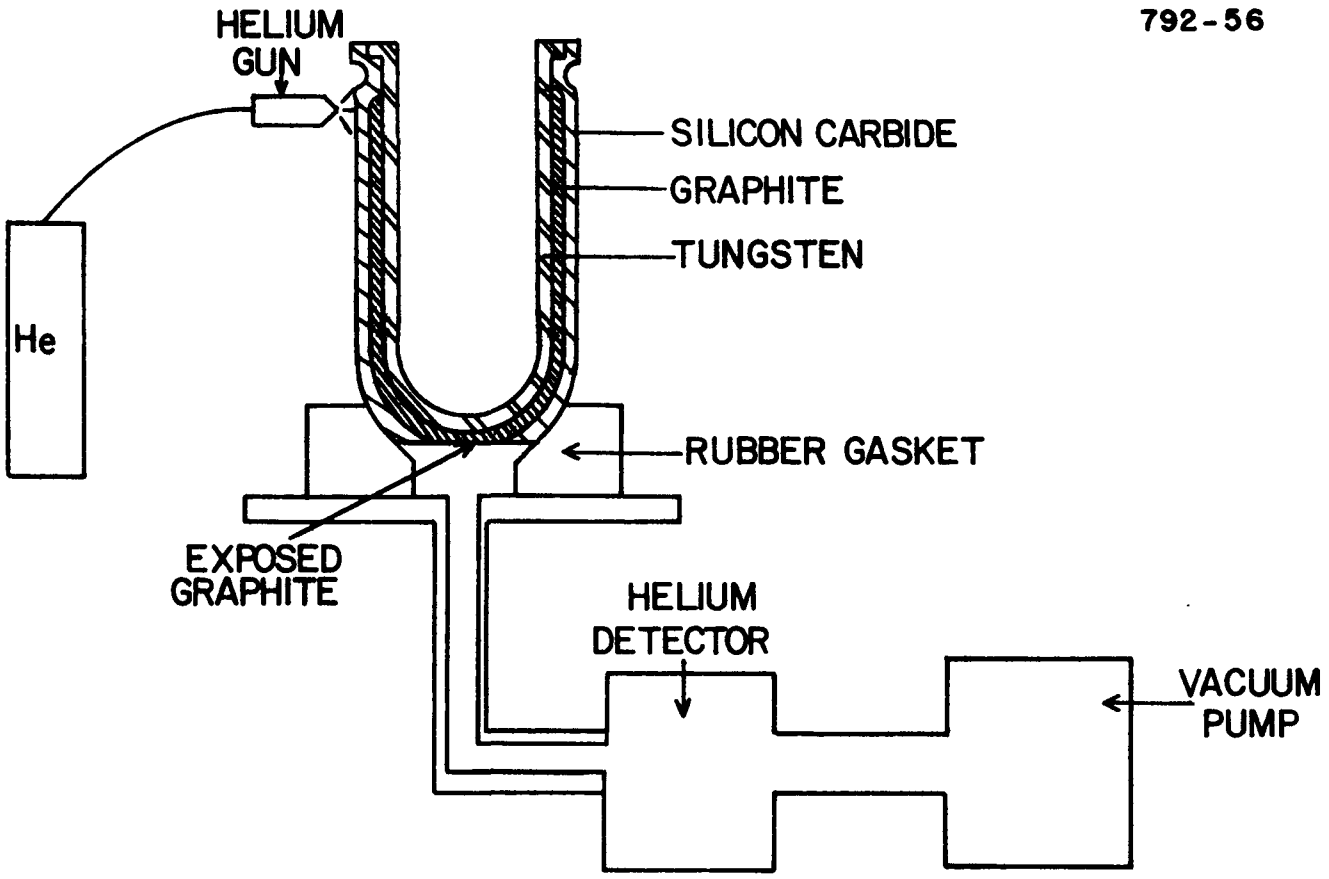

Figure 13. Destructive Leak Test Method

period. It is also possible either that the leak was intermittent or that the leak orginally detected was in the section of the shell that was machined off. This is an important test because the composite shell completely sealed the graphite but failed the helium soak test. This shell, which has silicon carbide deposited first and tungsten second, was cross-sectioned as shown in Figure 14. Although there was good bonding at the silicon carbide-tungsten interface, a gap was evident between the two materials on the outside. This may be the virtual leak that sorbed the helium during the soak period of the composite shell.

A composite shell with a molybdenum sleeve (which passed the "sniffer" tests, but not the helium soak test) was also cross-sectioned (see Figure 15). There was an obvious void between the sleeve and graphite, which can be corrected with a smaller tolerance between the graphite and molybdenum sleeve.

B. ALLOY HOT SHELL DEVELOPMENT

In order to improve the safety and prevent accidental temperature excursions of the simulated furnace, the combustion controls have been revised. Both an independent furnace controller and an over-temperature cutoff unit have been installed. A delay in component delivery from a vendor prevented furnace operation during this test period.

C. INTEGRAL CESIUM RESERVOIR CONVERTER NO. 208: TUNGSTEN EMITTER, NICKEL COLLECTOR CESIUM-GRAPHITE RESERVOIR

The design of this converter was described in the previous progress report. A 0.45-gram cylinder of POCO PLC-1 is used as the graphite reservoir. Initial performance data were taken to

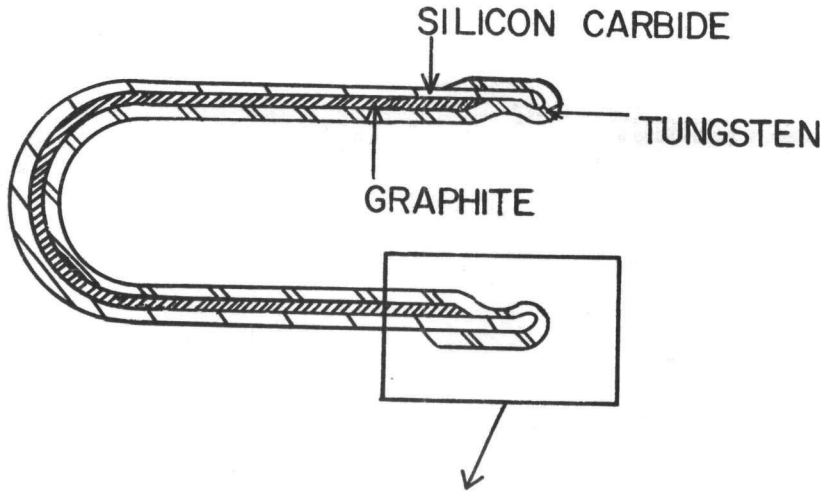

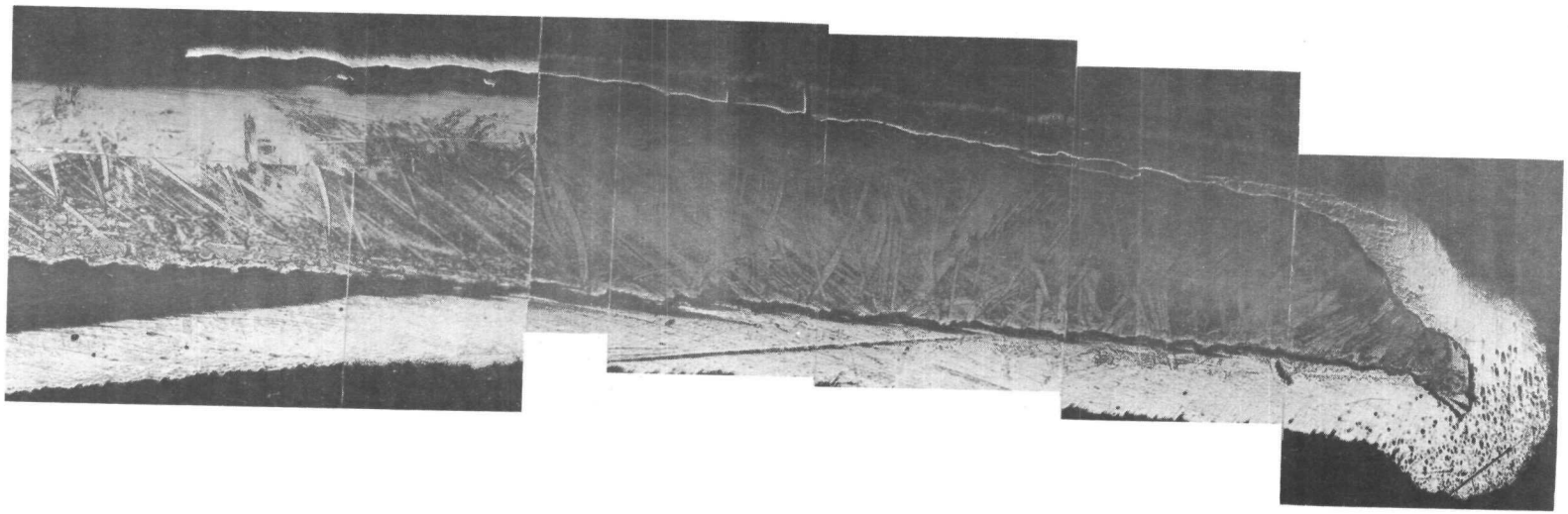

Figure 14. Cross Section of Composite Shell

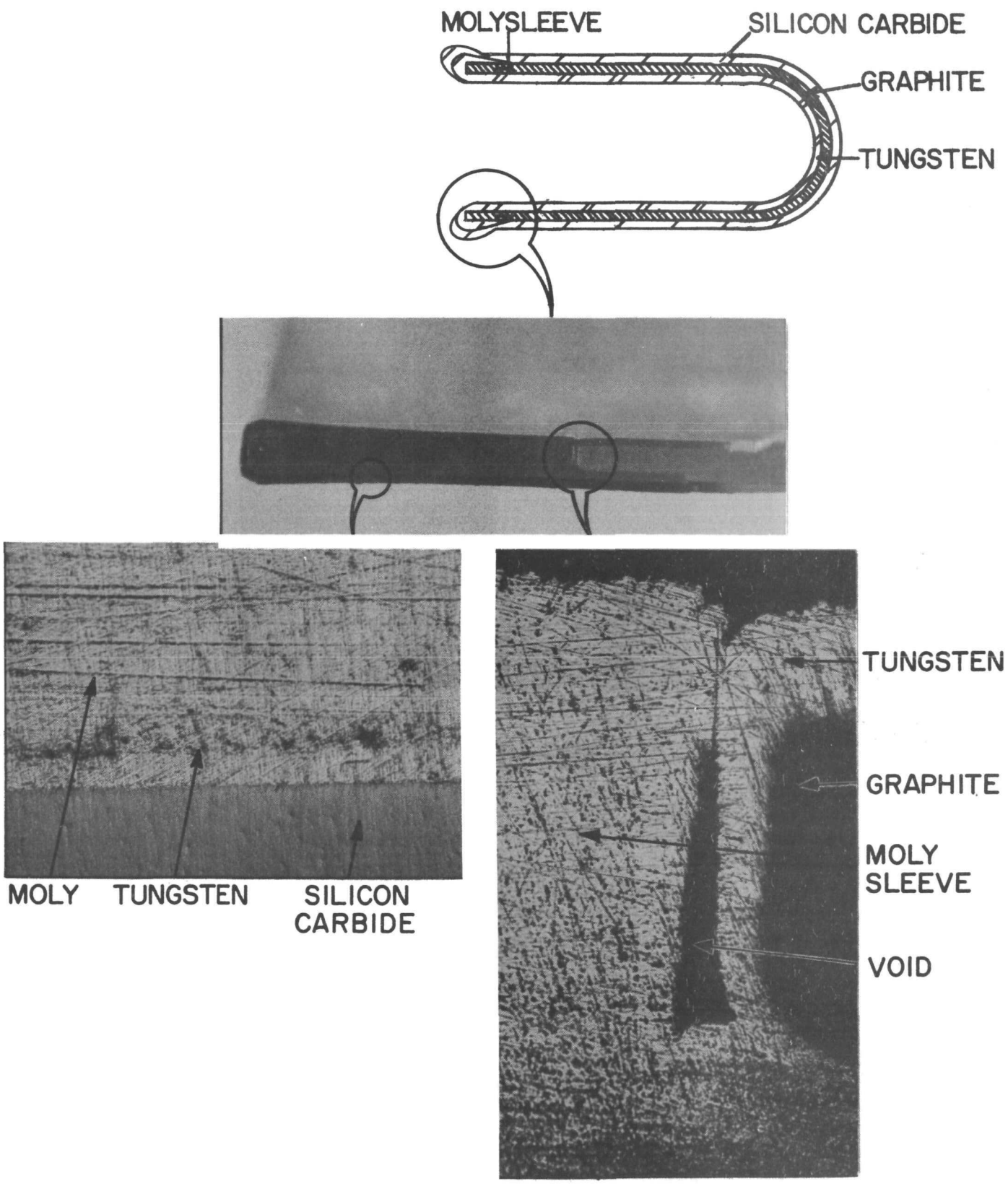

Figure 15. Cross Section of Composite Shell with Molybdenum Sleeve

characterize this converter. Cesium families were taken at emitter temperatures of 1400 and 1700 K. The spacing was optimized for each emitter temperature while the collector and cesium-graphite reservoir temperature was held constant at 750 K. A typical cesium family at 1700 K is shown in Figure 16. Saturation currents from these curves will be used to calibrate the cesium pressure above the cesium-graphite reservoir. It should be noted that, during all the initial testing, the graphite reservoir was exposed to the cesium vapor in the converter; thus, cesium-graphite compounds of different compositions were continuously formed.

After mapping the converter performance, several experiments were run prior to the final pinch off of the excess cesium. These studies were run to test the ability of the cesium-graphite reservoir to maintain adequate cesium pressure in the converter. In the first test, the cesium reservoir was cooled while the J-V characteristics were monitored. The cesium pressure dropped quite rapidly and the cesium-graphite reservoir appeared to have little or no effect. The cool cesium reservoir rapidly pumped any cesium that desorbed from the cesium-graphite reservoir. The second experiment was to vary the cesium-graphite reservoir temperature while all other parameters were held constant. No changes were observed in the converter performance, again indicating that the cesium reservoir determined the pressure in the converter.

After these tests, the converter was cooled and the copper tube connecting the liquid cesium reservoir to the converter was crimped. It was expected that, by crimping the tube to a small opening, the pumping speed of the liquid cesium reservoir would be slowed considerably.

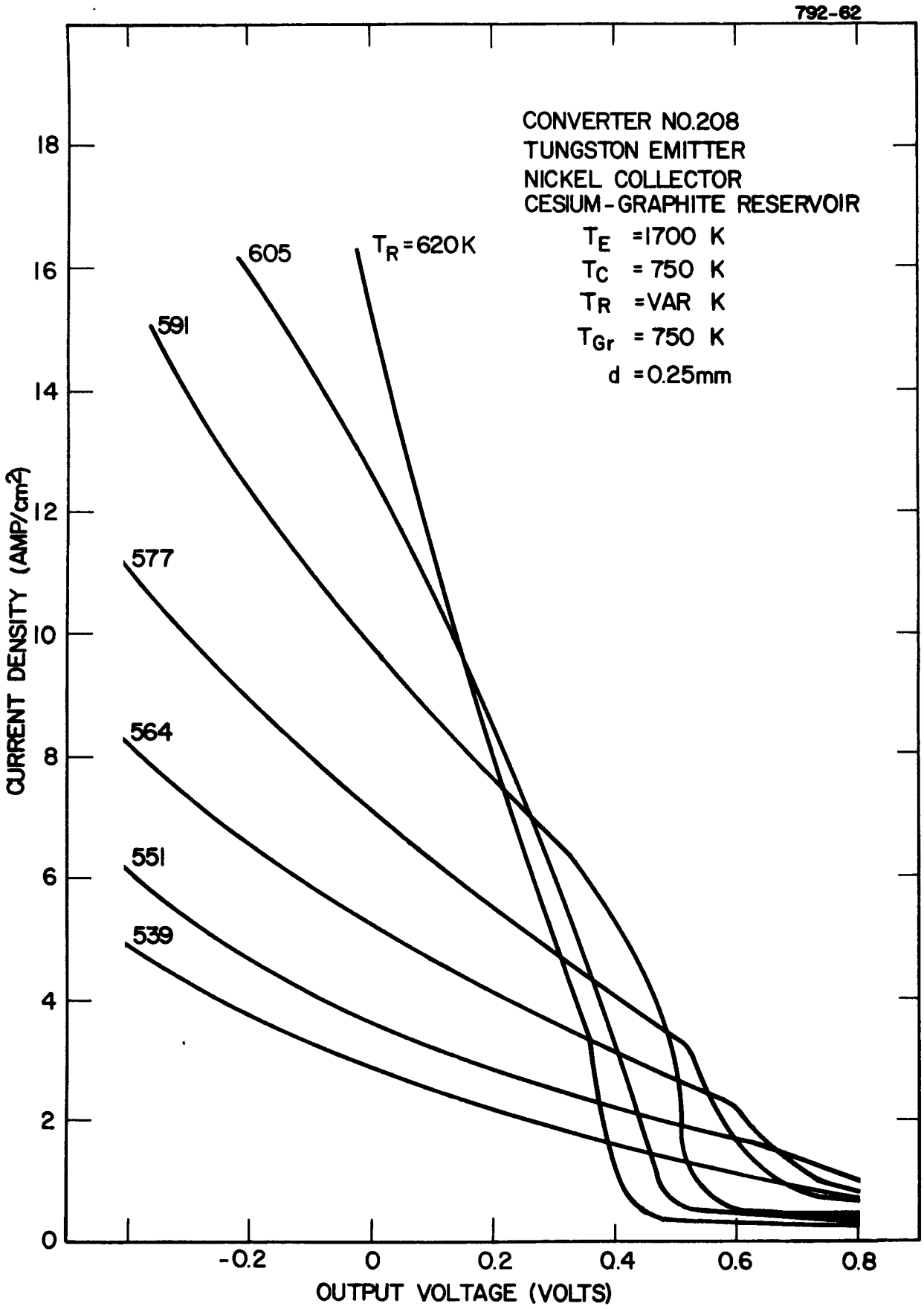

Figure 16. Typical Cesium Family

Both experiments described in the preceding paragraph were repeated. This time, the cesium-graphite reservoir had the anticipated effect on cesium pressure. After determining that the cesium-graphite reservoir could maintain adequate cesium pressure in the converter, the graphite was heated to 800 K and exposed to 2 torr of cesium for 48 hours. Next, the converter was cooled and the excess cesium was pinched off. Approximately 0.5 grams of cesium had reacted with the graphite (indicating a cesium-to-graphite weight ratio of 1:1).

The converter performance data were repeated using the cesium-graphite reservoir. Cesium families were taken again at emitter temperatures of 1400 and 1700 K. These results are shown in Figures 17 and 18.

The cesium pressure in the converter for a given cesium-graphite reservoir temperature was inferred by comparing the saturation currents with those of the initial data. The correlation of cesium pressure versus cesium-graphite reservoir temperature is given in Figure 19. Also plotted on this curve is the cesium pressure versus the liquid cesium reservoir temperature. Note that the sensitivities of both reservoirs (i.e., the cesium pressure change for a given temperature difference of the reservoir) are almost identical. The major difference between the reservoirs is that the graphite-cesium operates at a higher temperature.

Since calibrating the reservoir, the converter has been operated for 300 hours at the following conditions: $T_E = 1500$ K, $T_C = 750$ K, $T_{Graph/Cs} = 768$ K, and $d = 0.25$ mm. No significant change in converter performance has been apparent.

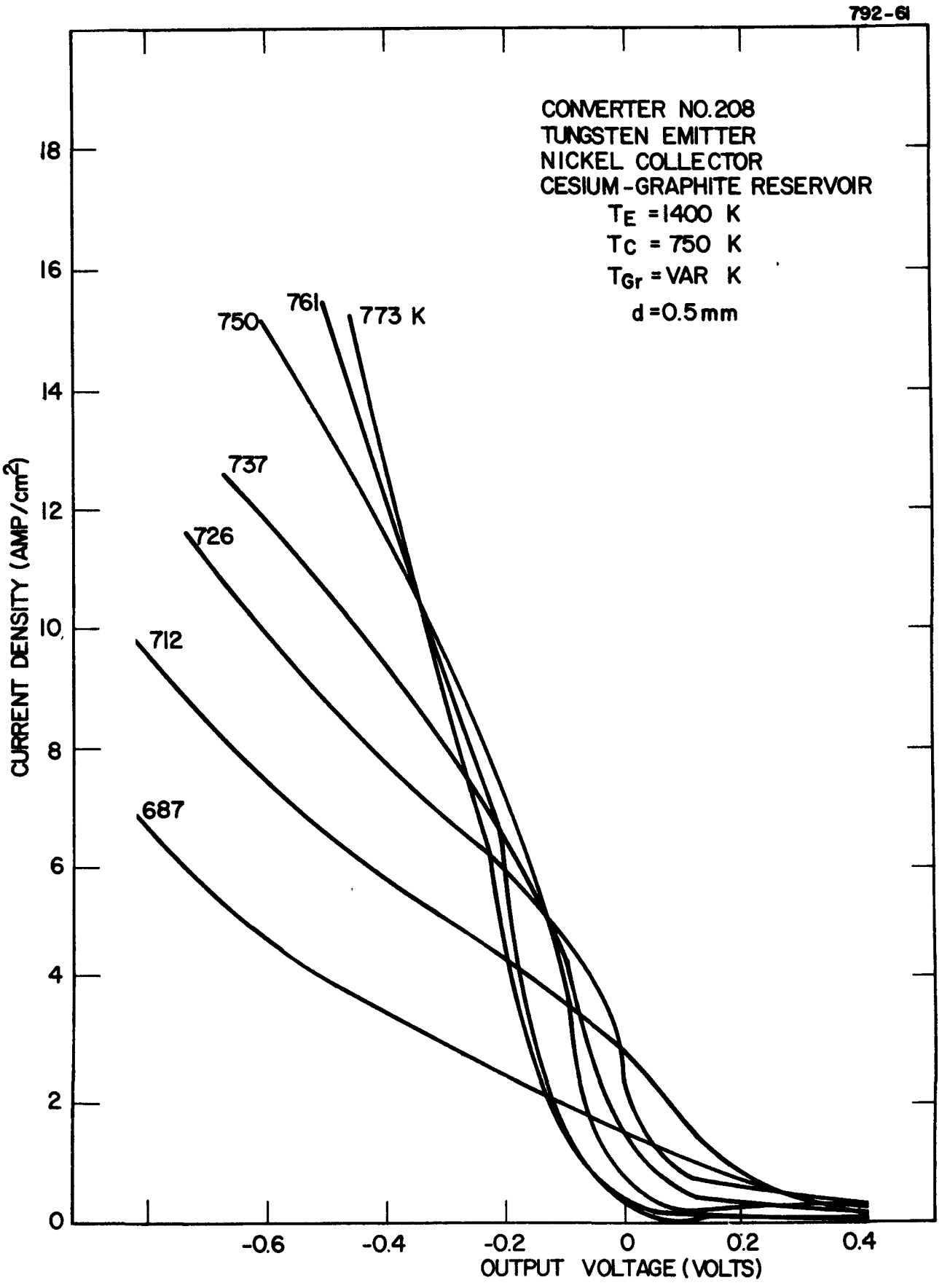

Figure 17. Cesium Family with Cesium-Graphite Reservoir, T_E = 1400 K

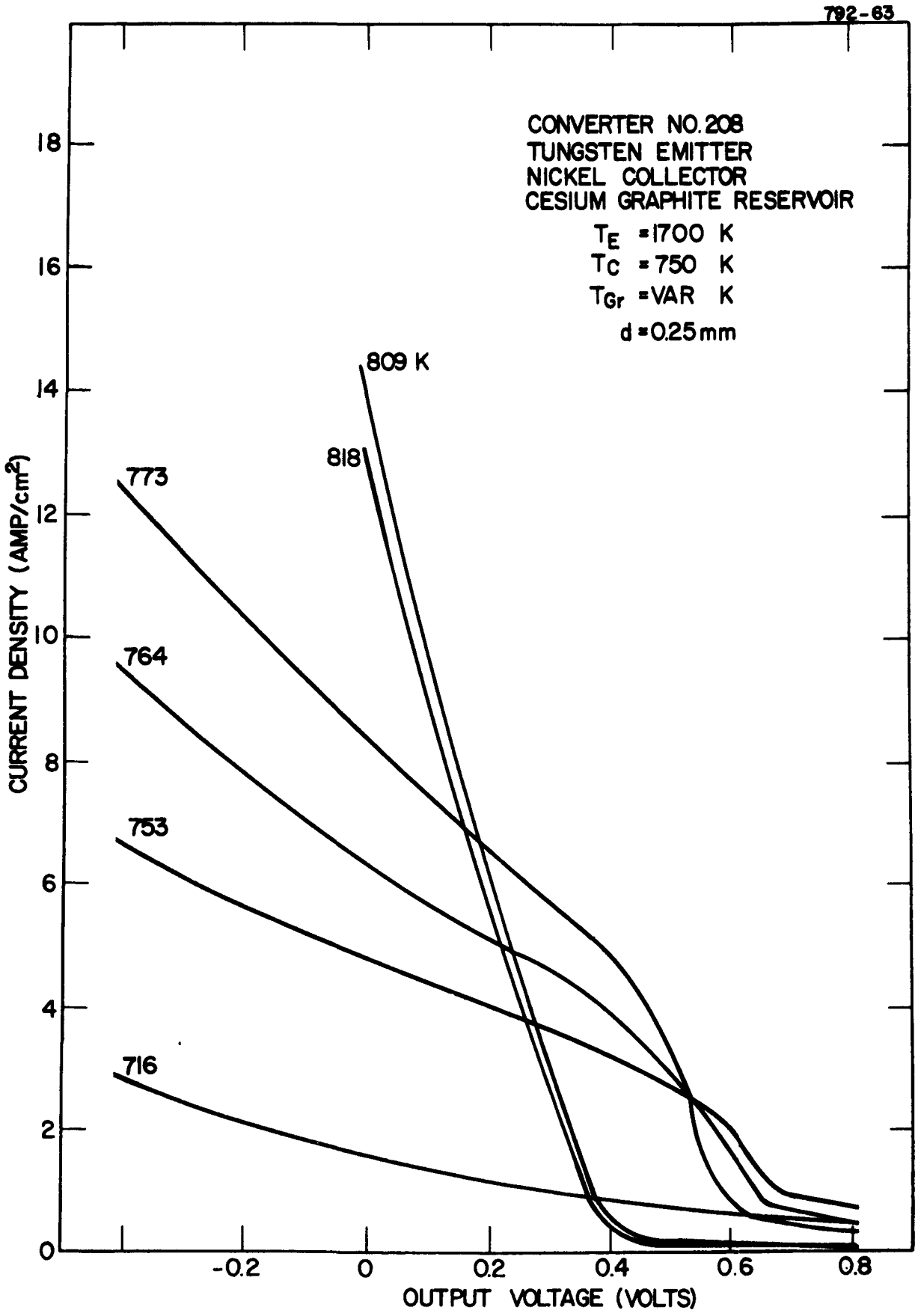

Figure 18. Cesium Family with Cesium-Graphite Reservoir, T_E = 1700 K

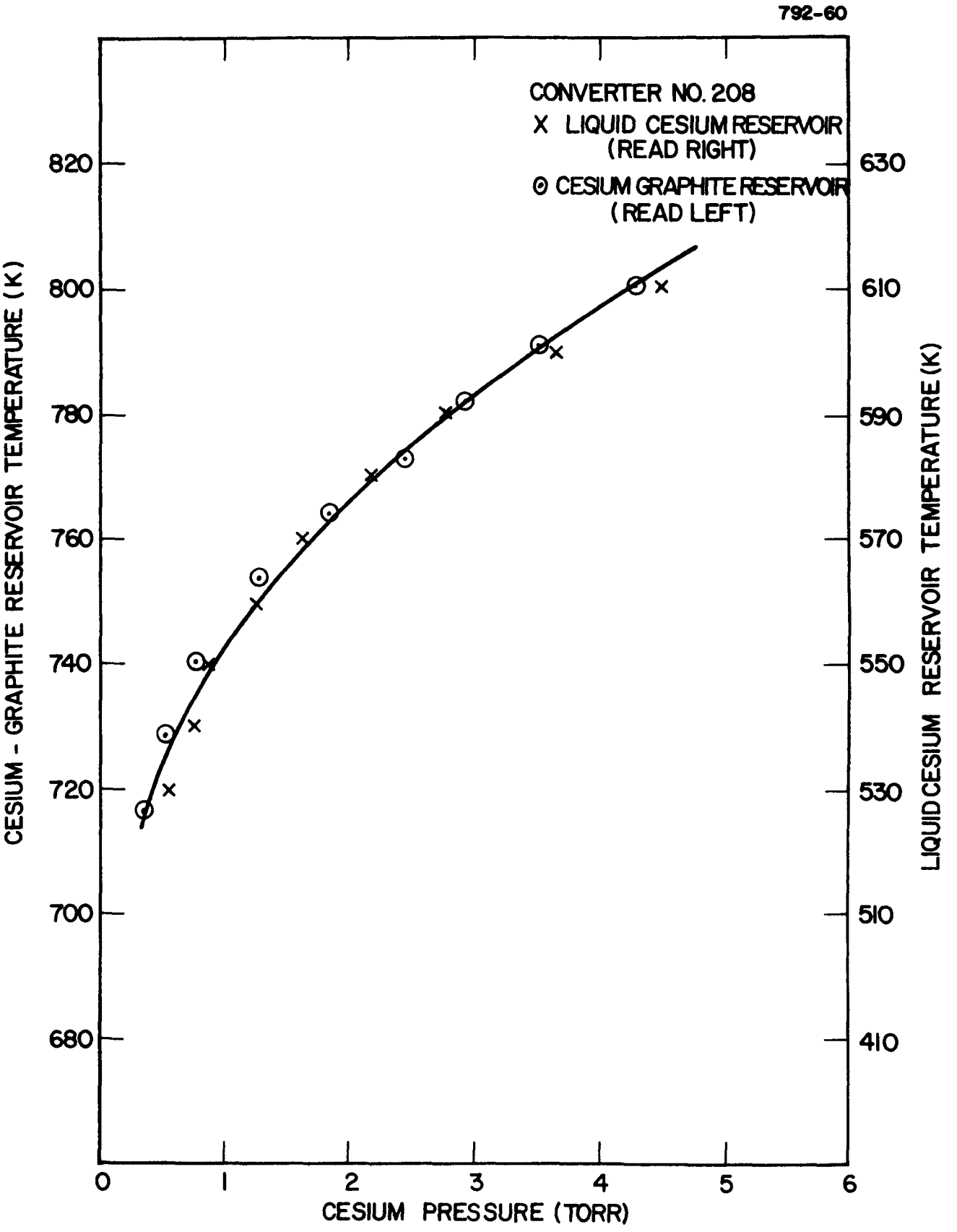

Figure 19. Cesium and Cesium-Graphite Reservoir Vapor Pressure Curve

During the next reporting period, this converter will be installed in a life test station and the performance will be monitored for long-term stability.

IV. COMBUSTION-HEATED THERMIONIC DEVICE

A. PROTOTYPE DEVICE NO. 1 (CONVERTER NO. 211)

The testing of Prototype Device No. 1 (see photograph of component in Figure 20) was concluded because the converter developed a leak due to a cracked ceramic in the ceramic-to-metal seal. Prior to the failure, an operating time of 432 hours was accumulated at an average temperature of 1370 K.

B. PROTOTYPE DEVICE NO. 2

The combustion-heated thermionic device was redesigned (see Figure 21). The primary modification was to the ceramic-to-metal seal geometry. The metal flanges mating to the ceramic were made thinner to minimize the differential thermal expansion stress. A heat shield was added to the ceramic-to-metal seal to reduce its temperature and to prevent evaporation of metal vapors onto the ceramic.

The collector cooling method was also revised. The potassium heat pipe collector cooling stem was replaced by a direct gas-cooled collector cavity. This change represents a closer approach to the current design of the thermionic converter for central station topping.

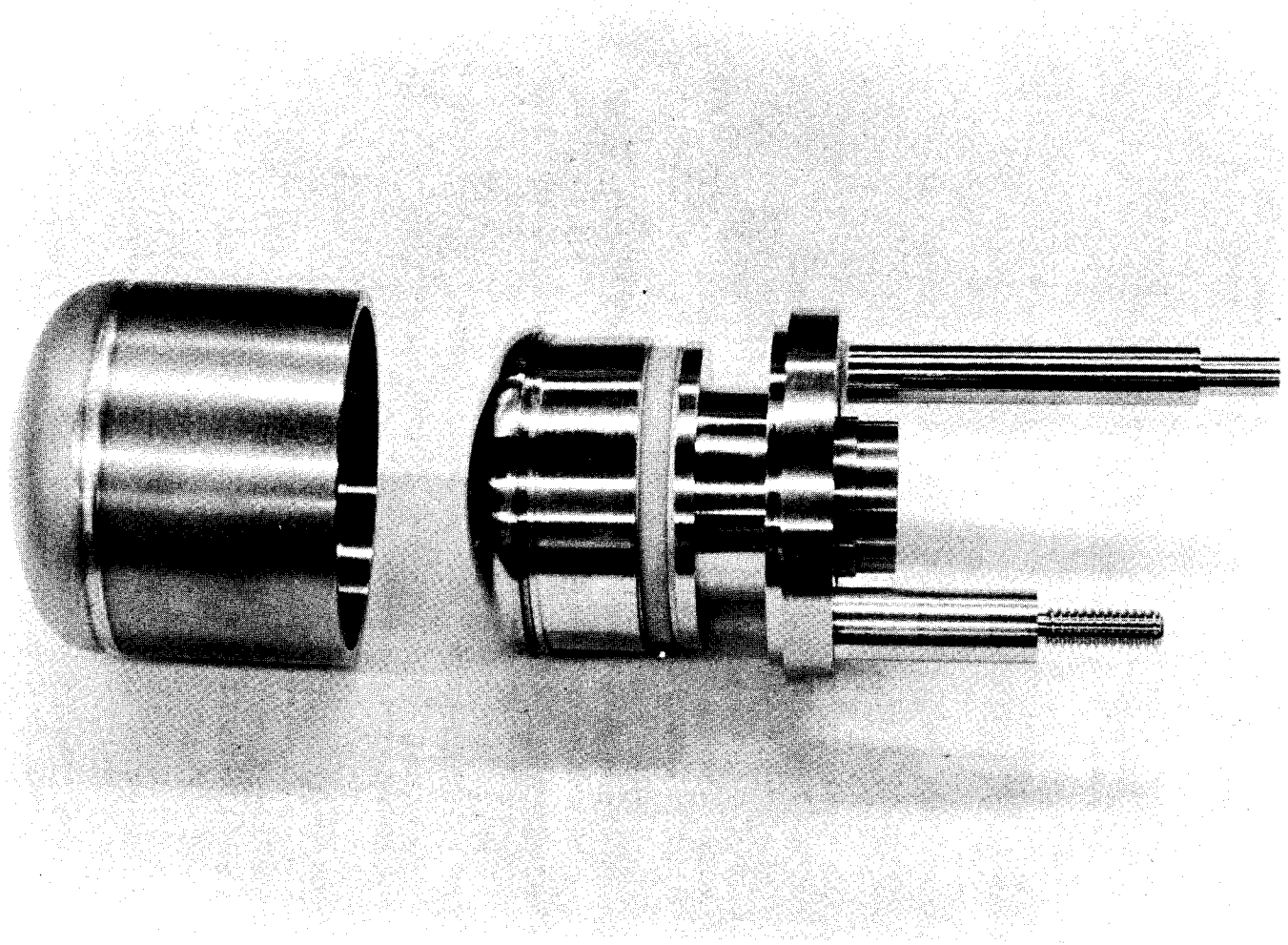

Figure 20. Photograph of Prototype Device No. 2 Prior to Assembly

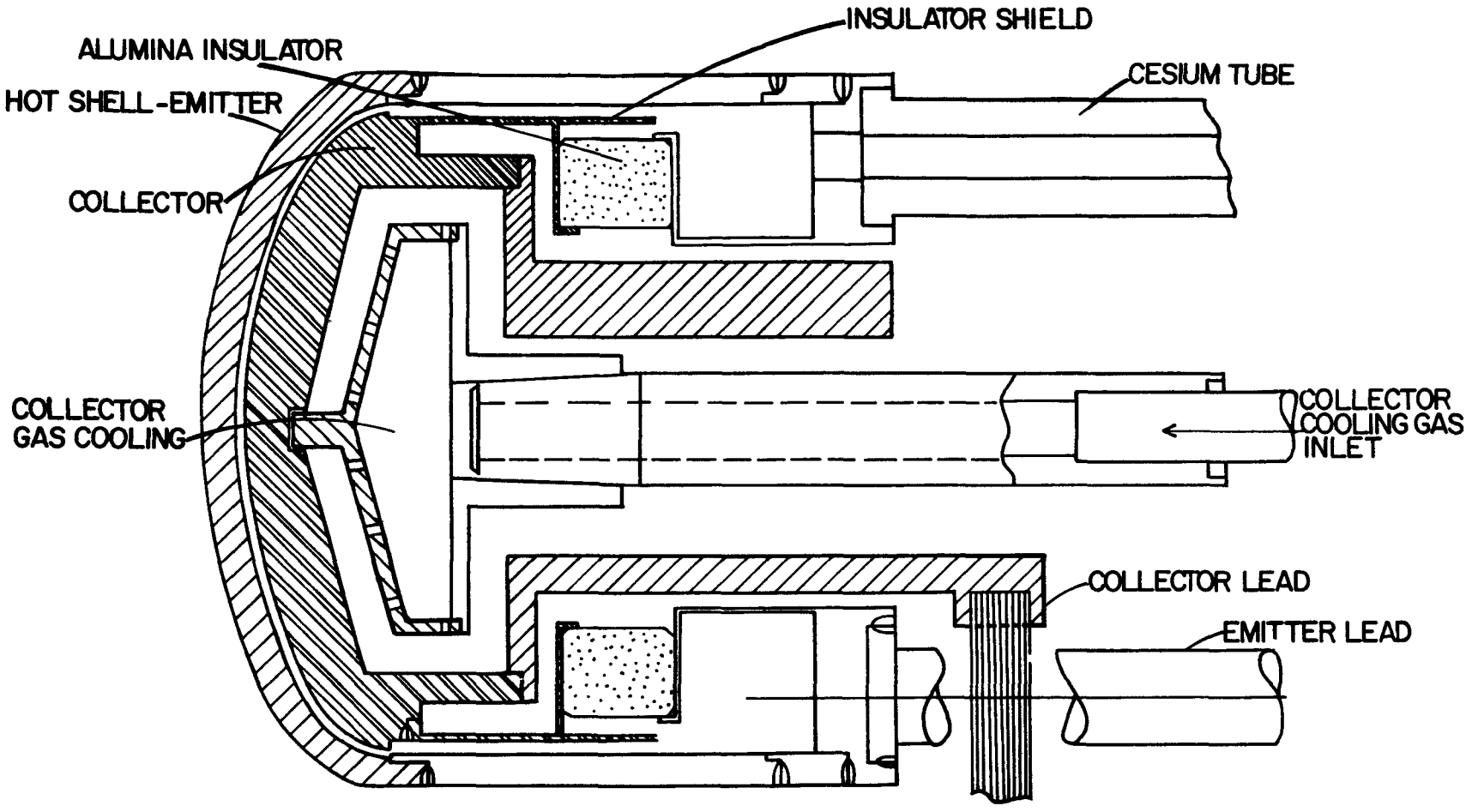

Figure 21. Cross Section of Prototype Device No. 2

PART TWO: JPL TASKS

I. BASIC SURFACE EXPERIMENTS

A. MOLYBDENUM OXIDE COLLECTOR SURFACE STUDIES

A new, double-walled, water-cooled sublimation furnace was designed and constructed. A series of baffles between the walls directs the flow of coolant to ensure maximum heat transfer from the samples. The configuration allows simultaneous depositions to be made on four collector surfaces, each of which can be independently positioned with respect to the hot, central molybdenum rod. An ionization gauge connected to the structure measures vacuum and low oxygen pressures directly inside the furnace. Oxygen is admitted into the sublimation enclosure by a circle of orifices that surrounds the molybdenum rod at the bottom of the furnace. Visual observation of the surfaces during deposition is possible through a series of skewed holes drilled through the cover plate on the furnace. The rigid construction of this furnace and its flexible current leads reduce, to a minimum, the bending of the heated molybdenum rod due to thermal expansion. Such distortion had appreciably changed the critical rod-to-collector separations during sublimation runs in the previously used furnace.

In an initial test, both niobium and molybdenum substrates were simultaneously coated with molybdenum sublimed from a rod heated to 2380 K in oxygen at a pressure of 4×10^{-5} torr. These conditions produced high surface oxygen concentrations (approximately 20,000 ppm), which were a factor of four-to-five times higher than previously measured. These results indicate that the oxygen penetration into the enclosure of the old furnace had been relatively poor.

B. ADJUSTABLE CESIUM PRESSURE ACTIVATION CHAMBER

A molybdenum sample was tested in ACPAC during this reporting period. The work function was measured at a sample temperature of 650 K and cesium reservoir temperatures of 396 to 488 K. The glass envelope leaked to atmosphere shortly after testing was initiated and only four data points were obtained. However, as shown in Figure 22, these points show a good correlation with previously obtained molybdenum data from converters.

This was the first test with the redesigned ACPAC, and the results were quite encouraging. The filament heater worked well. Samples could easily be heated to, and held at, any temperature up to 1000 K. The cesium pressure in the chamber could be varied between 1×10^{-3} and 5×10^{-2} torr. Leakage resistance between the electrodes was greater than 10^{7} ohms at all cesium pressures.

The leak in the glass envelope was due to a crack near the glass to kovar seal and was probably caused by excessive mechanical stress while the glass was at elevated temperatures. This problem should be eliminated by modifying the test arrangement to relieve the mechanical stresses. A new glass enevelope has been ordered.

C. SURFACE CHARACTERIZATION CHAMBER

The characterization of iridium surfaces with coadsorbed cesium and oxygen was completed during this reporting period. Work functions (FERP method), reflection coefficients (FERP method), and surface compositions (Auger analysis) were measured for a wide range of cesium and oxygen coverages.

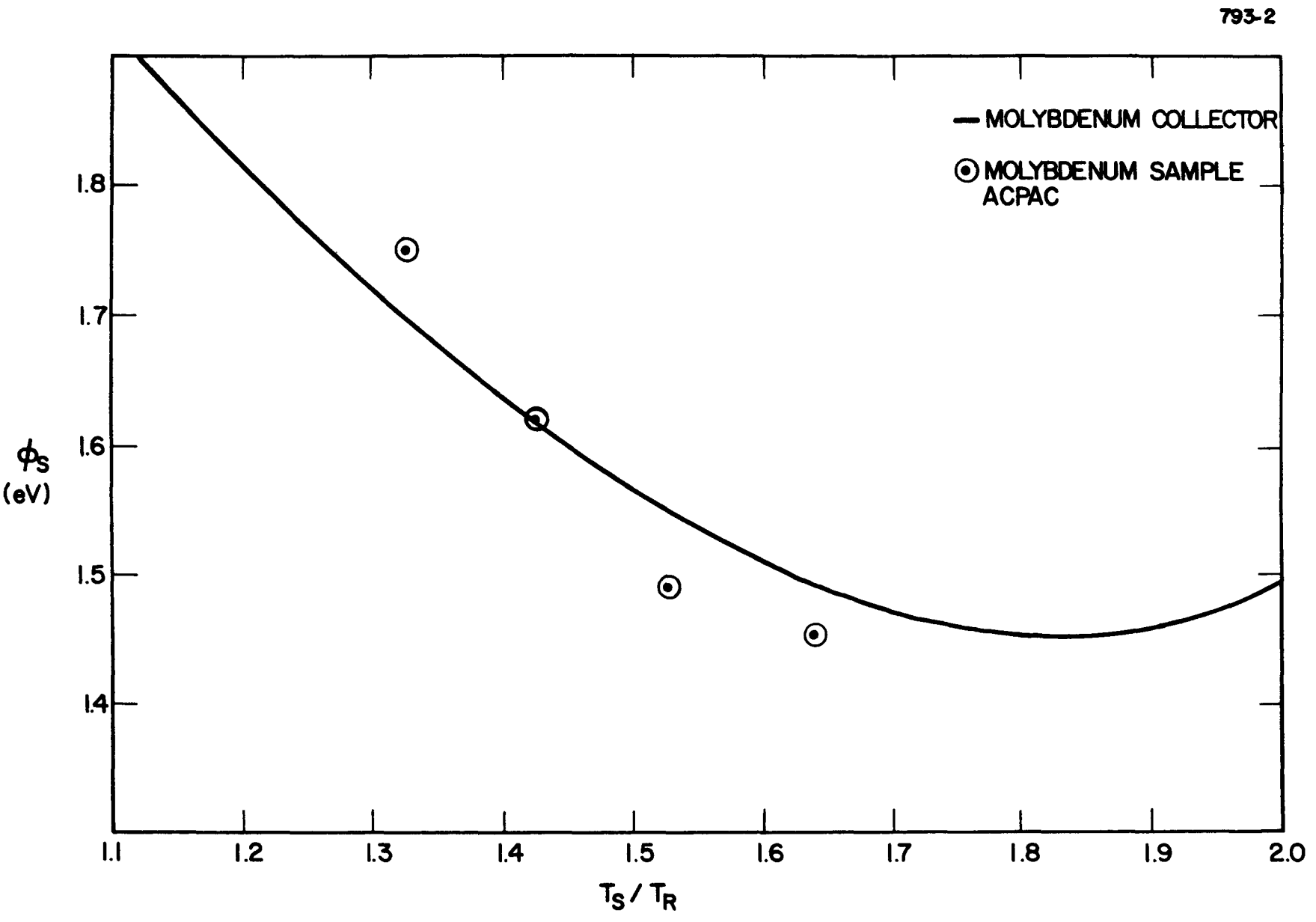

Figure 22. Comparison of the Work Function of a Molybdenum Sample with a Molybdenum Collector versus the Ratio of Sample Temperature to Cesium Reservoir Temperature

The polycrystalline iridium sample was cleaned initially and prior to each experiment by argon ion sputtering. Typical impurity levels at the beginning of a run were carbon (<6%), nitrogen (<3%), cesium (<2%), and oxygen (<1%). FERP work functions for such a surface ranged from 5.0 to 5.6 eV, probably due to the small impurity concentrations.

Reproducible, oxygen-free cesium doses were provided by a cesium channel mounted inside the vacuum system. All cesium doses were identical (30 sec, 4.5 A through channel after 2-min warm-up). The FERP work function (ϕ) and percent coverage of iridium, cesium, oxygen, carbon and nitrogen as a function of cesium doses is shown in Figure 23. The work function drops to 1.6 eV after four cesium doses. Figure 24 gives I (collector current) versus V (collector voltage) for this cesiated surface and for a clean iridium surface. Comparison of the first maximum peaks shows a reflection of only 18% for the cesiated, compared to the clean, surface. Thus a pure cesium coverage does not produce a high reflectivity, even with a work function of 1.6 eV.

The effect of oxygen on a cesium overlayer was studied in two ways. First, the cesiated iridium surface was exposed to 7.2×10^{-6} torr-sec of oxygen. The work function increased from 1.6 eV to 2.8 eV, as shown in Figure 23. A subsequent cesium dose reduced the work function slightly to 2.5 eV. Continued alternation of oxygen and cesium doses would probably lead to a low work function surface. However, a second oxygen dosing technique yielded a faster way to obtain a low work function surface.

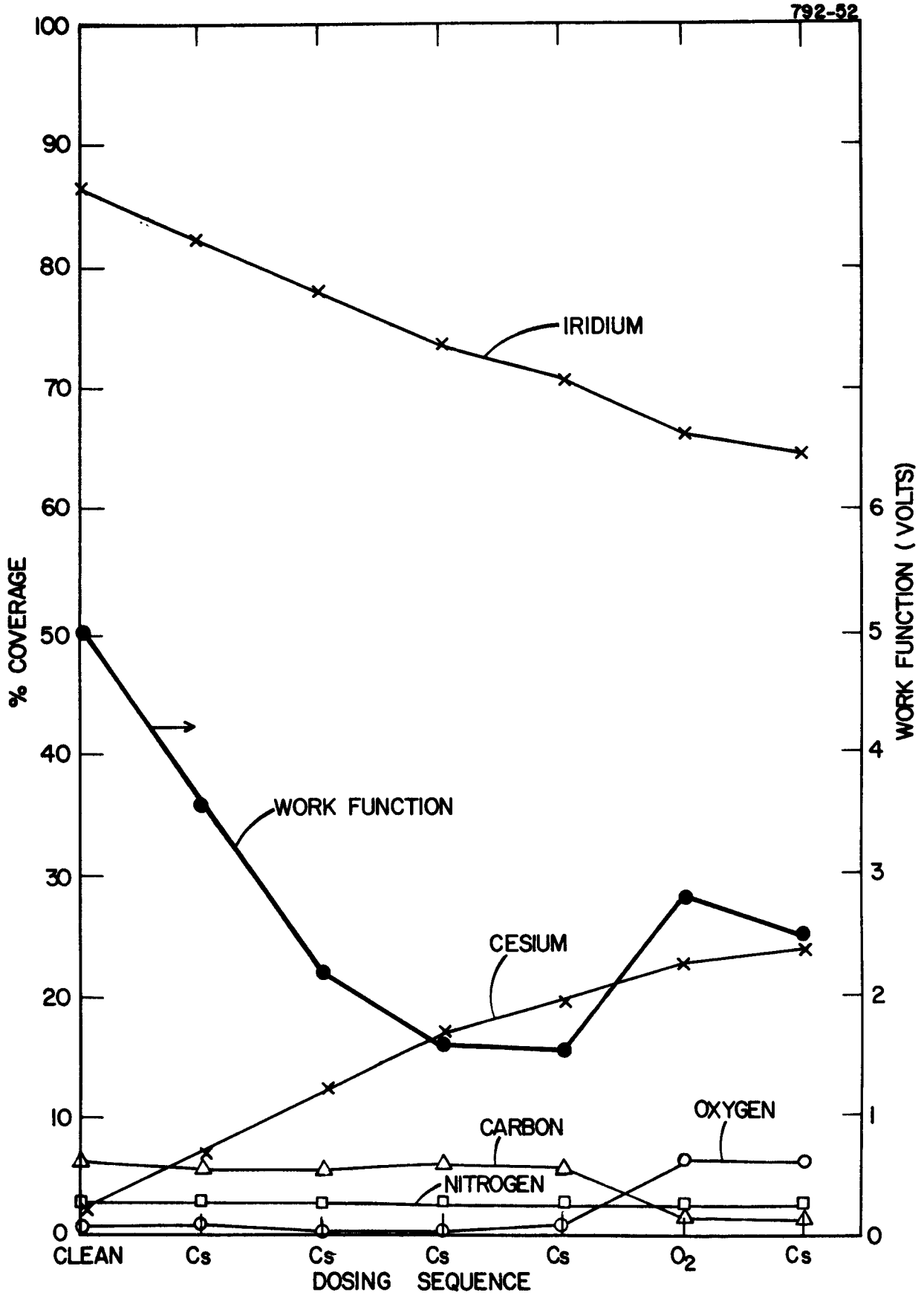

Figure 23. Work Function and Percent Coverages for Cesium and Oxygen Doses on Polycrystalline Iridium

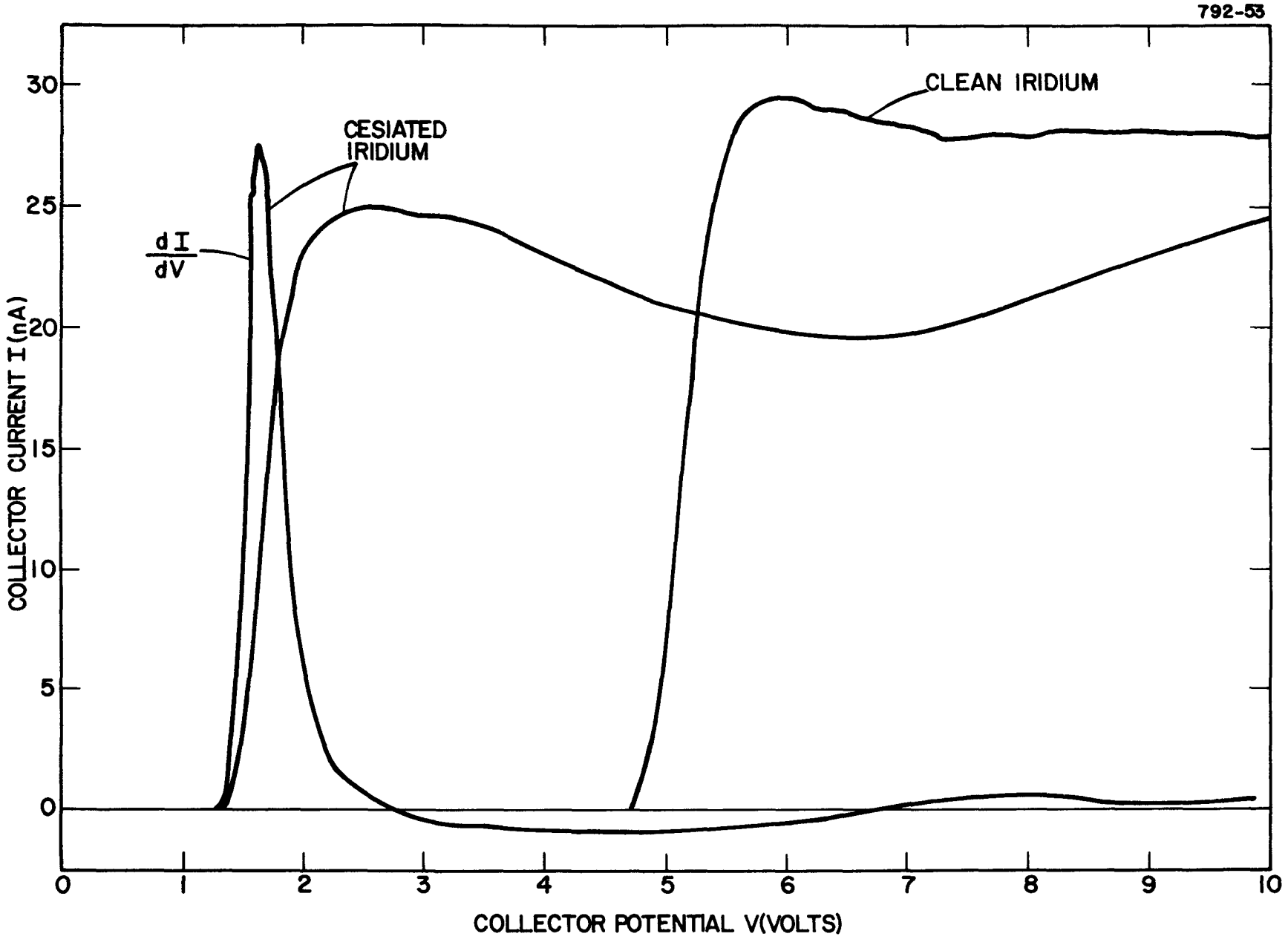

Figure 24. Cesium on Iridium, Collector Current versus Collector Voltage (FERP Technique)

This second method is to dose a clean iridium surface with cesium until ϕ = 1.6 eV is obtained and then simultaneously dose with cesium and oxygen (P = 5 x 10^{-9} torr). The photoemission current increases with time until a maximum is obtained. Figure 25 shows dI/dV curves for the surface after maximum photoemission is achieved. The minimum work function is 1.05 eV and other peaks correspond to ϕ = 1.25, 3.48, and 4.80 eV. A previous similar (but shorter) run gave ϕ = 0.95, 3.50, and 4.8 eV, with no peak at 1.25 eV. Apparently cesium-oxygen patches of different work functions are formed on the surface, and formation of these patches is sensitive to the dosing technique. Comparison of the current at the first maxima of the clean and cesium-oxygen surfaces gives a reflectivity of 63%, significantly larger than the value of 18% obtained for a cesium layer alone.

A summary of work functions, reflectivities, and surface coverages for cesium and cesium plus oxygen on polycrystalline iridium is given in Table I. The very low iridium coverage for the 1.0-eV work function is notable. The escape depth for 1900-V Auger electrons is about 20 Å. This implies that the cesium-oxygen layer for this 1.0-eV surface is 20 Å thick. By contrast, the cesium layer for this 1.6-eV surface is probably only 1 to 3 Å thick.

II. TRIODE CONVERTER EXPERIMENTS

In the last progress report, the characteristics of the pulse triode filled with xenon were summarized. During this reporting period, the investigation of the triode was completed using both cesium vapor and xenon gas in the converter.

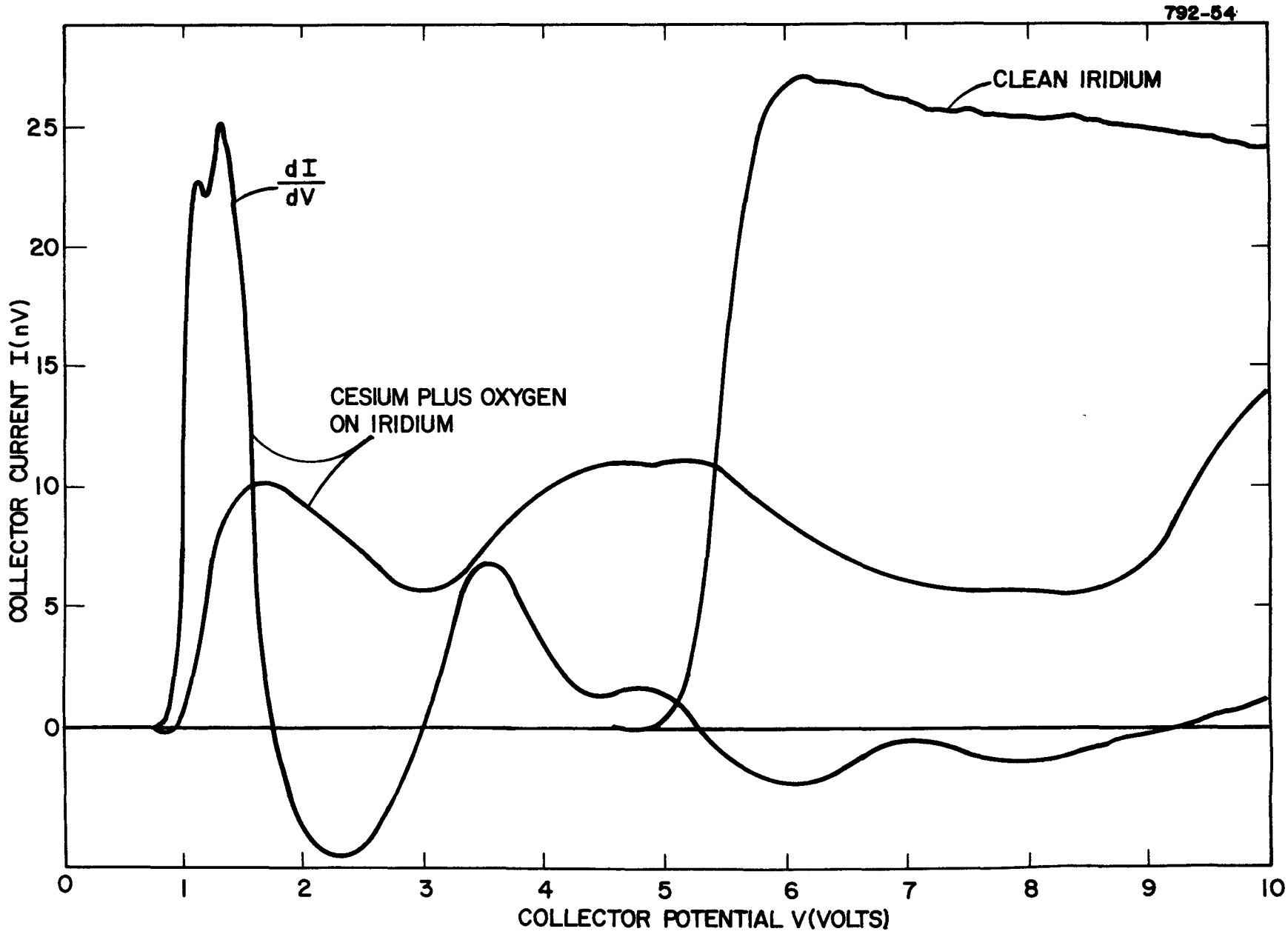

Figure 25. Cesium Plus Oxygen on Iridium Collector Current versus Collector Voltage (FERP Technique)

TABLE I

SUMMARY OF IRIDIUM DATA

PROPERTIES	CESIUM	CESIUM PLUS OXYGEN
Minimum Work Function	1.6 eV	1.0 eV
Reflection Coefficient (at first max)	0.18	1.63
Surface Coverages*		
Cs_{563}	19%	80%
O_{510}	1%	14%
Ir_{1908}	69%	6%
C_{273}	8%	0%
N_{380}	3%	0%

*Subscripts on elements denote energy of Auger peak used to calculate coverages.

Representative current trace results from single pulse experiments as a function of xenon pressure are shown in Figure 26. Figure 27 shows selected J-V characteristics of the triode as a function of xenon pressure under the condition of constant pulse power input. It is concluded that the highest power output is obtained when the triode is filled with low cesium pressure and high xenon pressure.

Direct comparison between the diode and triode is difficult because the geometry, the operating conditions, and the output form between the two are different. The diode favors high cesium pressure (1 torr and larger), and narrow spacing (10 mils and less), and the output is direct current. The triode, on the other hand, favors low cesium pressure with high xenon pressure and larger spacing (100 mils), and the output is alternating current. Operating the triode converter in the pulse condition gives better results than operating the converter in the diode configuration, counting in the pulse power expenditure. The experiments were terminated when the triode converter developed a window leak during the final stage of testing. The triode will be cut open and examined.

III. DESIGN OF CYLINDRICAL CONVERTER

A. HALF-LENGTH CONVERTER

The layout of the "half-length" cylindrical converter was shown in the last progress report.[2] This design has a semiconductor sleeve combined with a radial emitter-collector heat choke. A bellows-insulator assembly was also shown on the layout. Alternate configurations of both the emitter-collector heat choke and the bellows-insulator assembly were studied. Coordination with the overall system optimization is needed before the final design of these components can be selected.

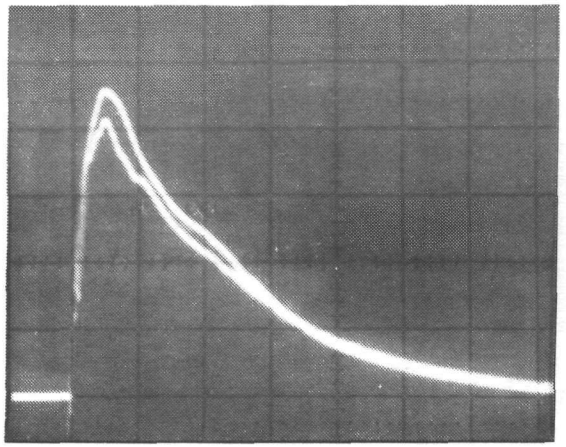

Xe 0 torr
t 20 μs/div

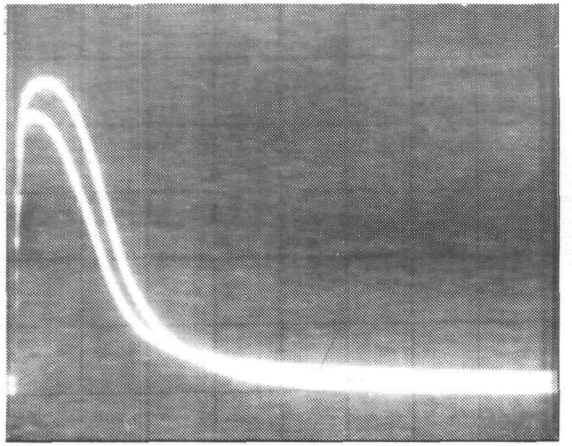

Xe 1 torr
t 0.1 ms/div

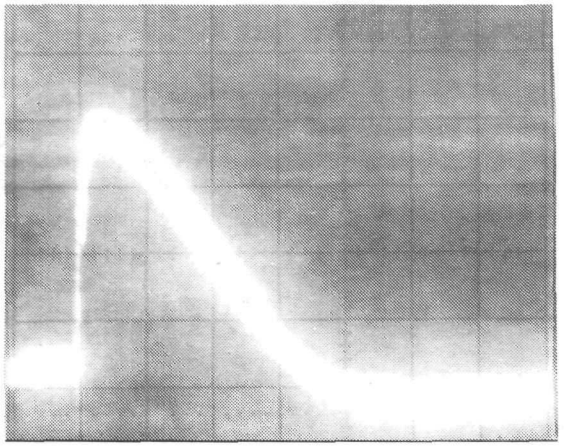

Xe 3 torr
t 0.1 ms/div

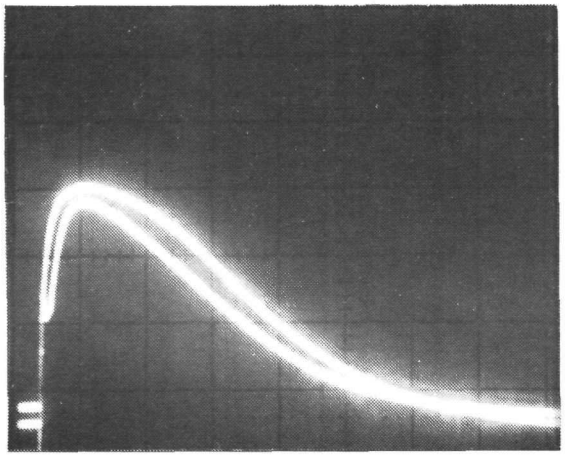

Xe 5 torr
t 0.1 ms/div

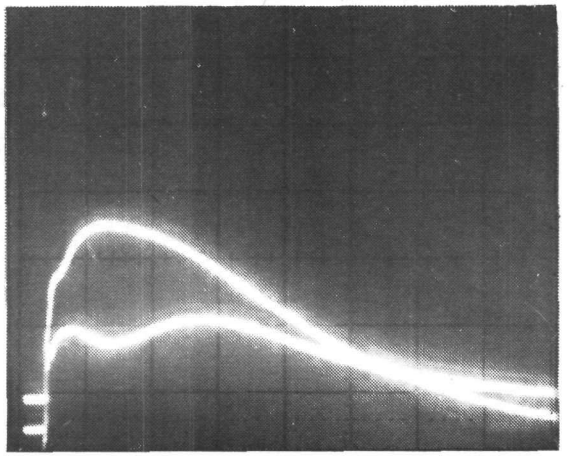

Xe 10 torr
t 0.1 ms/div

T_E	= 1400°K
T_C	= 503°K
I_C	= 20 mA/div
I_G	= 0.1 A/div
d	= 2 mm
Pulse	= 80 V
Bias	= 0 V
Cesium	= 10^{-3} torr

Figure 26. Transient Collector and Guard Currents, Parametric in Xenon Pressure. (Note: Higher Curves are Guard Current Traces).

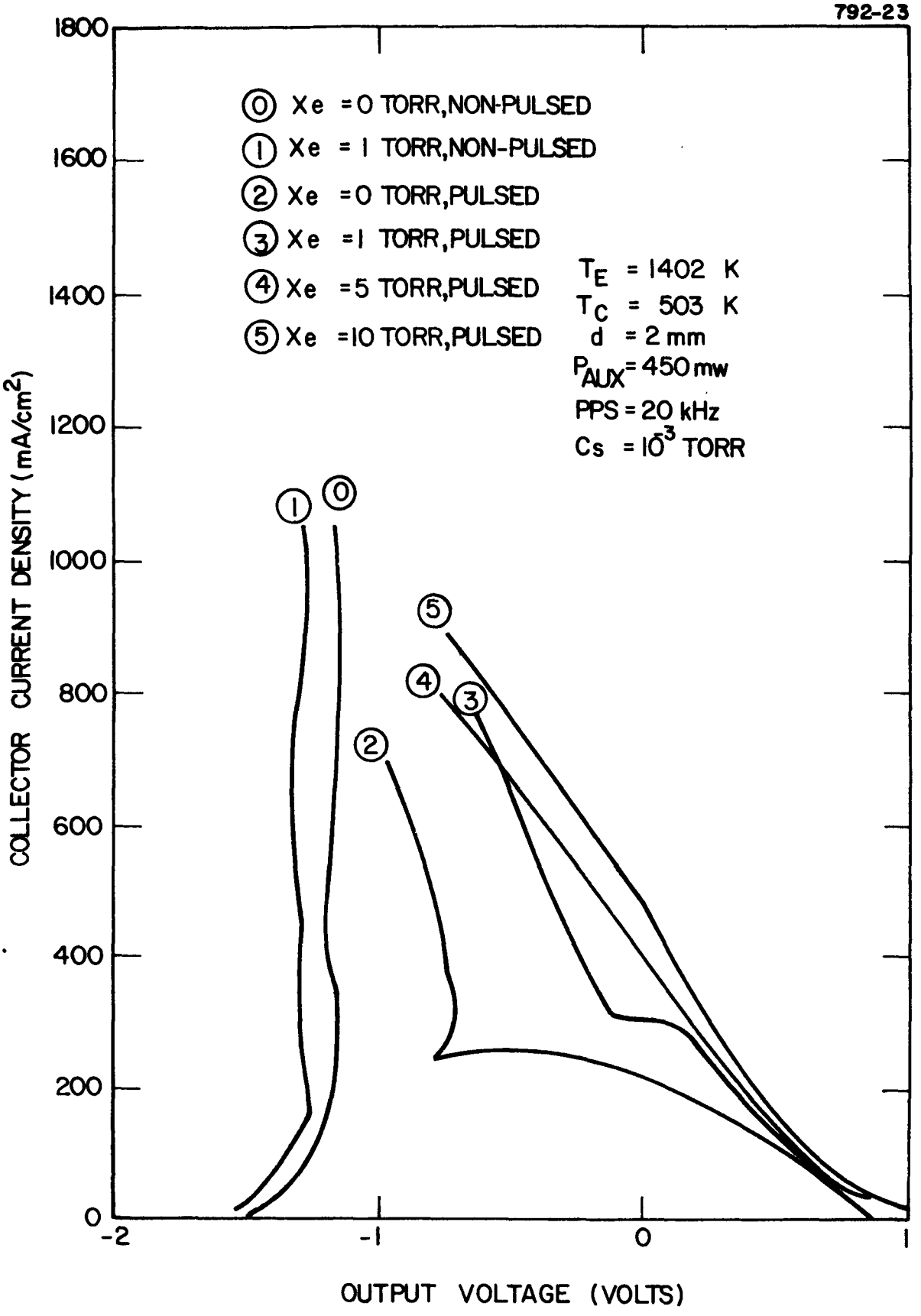

Figure 27. Guarded Triode Current Density-Voltage Characteristics, Parametric in Xenon Pressure

The alternate heat choke designs are shown in Figure 28. Figure 28A shows the tubular heat choke design. This type of heat choke is currently used on all research converters built at Thermo Electron. Prototypic cylindrical converters have also used tubular heat chokes. An alternate design of a radial heat choke is shown in Figure 28B. The radial design reduces the axial space required for the heat choke but represents a greater heat leak, for the same material thickness, than does a tubular design.

Two design concepts for the bellows-seal subassembly are shown in Figure 29. Figure 29A shows a planar bellows-seal. Such a seal is also currently used on a variable-spacing research converter built at Thermo Electron and can be fabricated with relatively simple tooling. A nested configuration, shown in Figure 29B requires less axial space for a given number of convolutions, but requires somewhat more complex tooling. Either of the alternative concepts can be incorporated into the design layout as dictated by the overall system requirements.

IV. HIGH-EFFICIENCY CONVERSION EXPERIMENTS

A. CONVERTER NO. 210: TUNGSTEN EMITTER, MOLYBDENUM OXIDE COLLECTOR

During initial testing, a partial electrical short between the collector and emitter at spacings of approximately 0.2 mm was noticed. This large minimum spacing made it impossible to measure the collector work function from retarding plots. Flaking of the molybdenum oxide coating probably caused this shorting. Power output measurements were therefore limited to minimum electrode spacings of 0.25 mm.

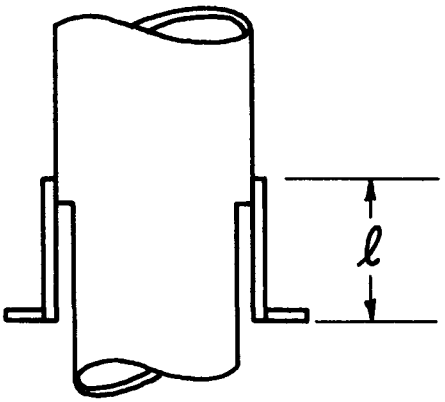

A) Tubular Heat Choke

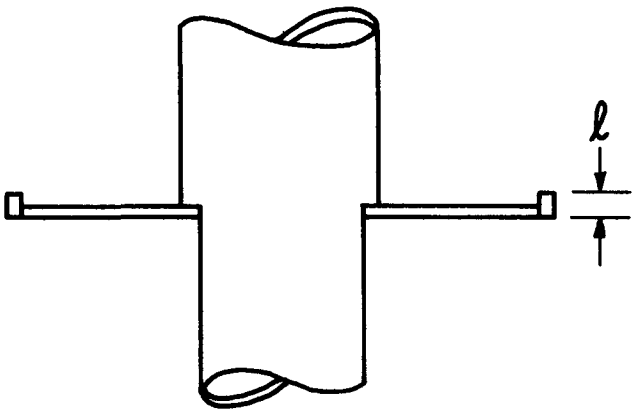

B) Radial Heat Choke

Figure 28. Emitter-Collector Heat Choke Designs

787-40

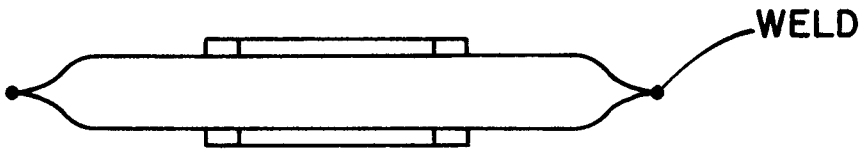

A) Planar Configuration

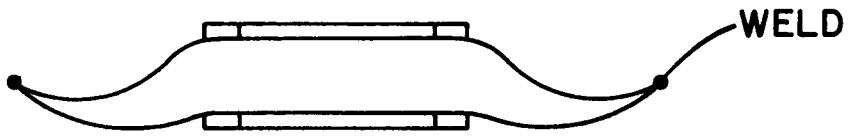

B) Nested Configuration

Figure 29. Bellows Concepts

The initial tests focused on investigating the effects on the emitter of dispensing oxygen from the collector. An increase in saturation current represents a lowering of emitter work function. A dependence of saturation current on collector temperature would indicate that an additive is available to lower the emitter work function and that its source is the collector. Over the collector temperature range of 600 to 750 K, saturation current was independent of collector temperature. However, at a collector temperature of 760 K, a time-dependent increase in saturation current was observed. This result is shown in Figure 30. Previous work by Pigford[3] indicates that, at 760 K, Mo_3O_9 volatilizes with a vapor pressure of about 10^{-5} torr. Liberation of oxygen at this pressure should account for the observed results.

The time dependency of the phenomenon suggests that chemical reactions are taking place. Earlier work at Thermo Electron[4] described two possible reactions in which cesium can reduce MoO_3 to produce the cesium oxide responsible for lowering the emitter work function. On the collector surface the following reaction may occur:

$$MoO_{3(s)} + 2Cs_{(g)} \leftrightarrows MoO_{2(s)} + Cs_2O_{(s)}$$

If the reaction occurs in the gas phase:

$$Mo_3O_{9(g)} + 6Cs_{(g)} \leftrightarrows 3MoO_{2(s)} + 3Cs_2O_{(l)}.$$

Conditions for both reactions are satisfied under normal operating conditions of the diode.

Performance data were taken at emitter temperatures of 1400 and 1600 K. A typical cesium family for the converter is given in Figure 31. Figures 32 and 33 show the cesium-optimized performance at several interelectrode spacings. At 6 A/cm^2 the barrier indices

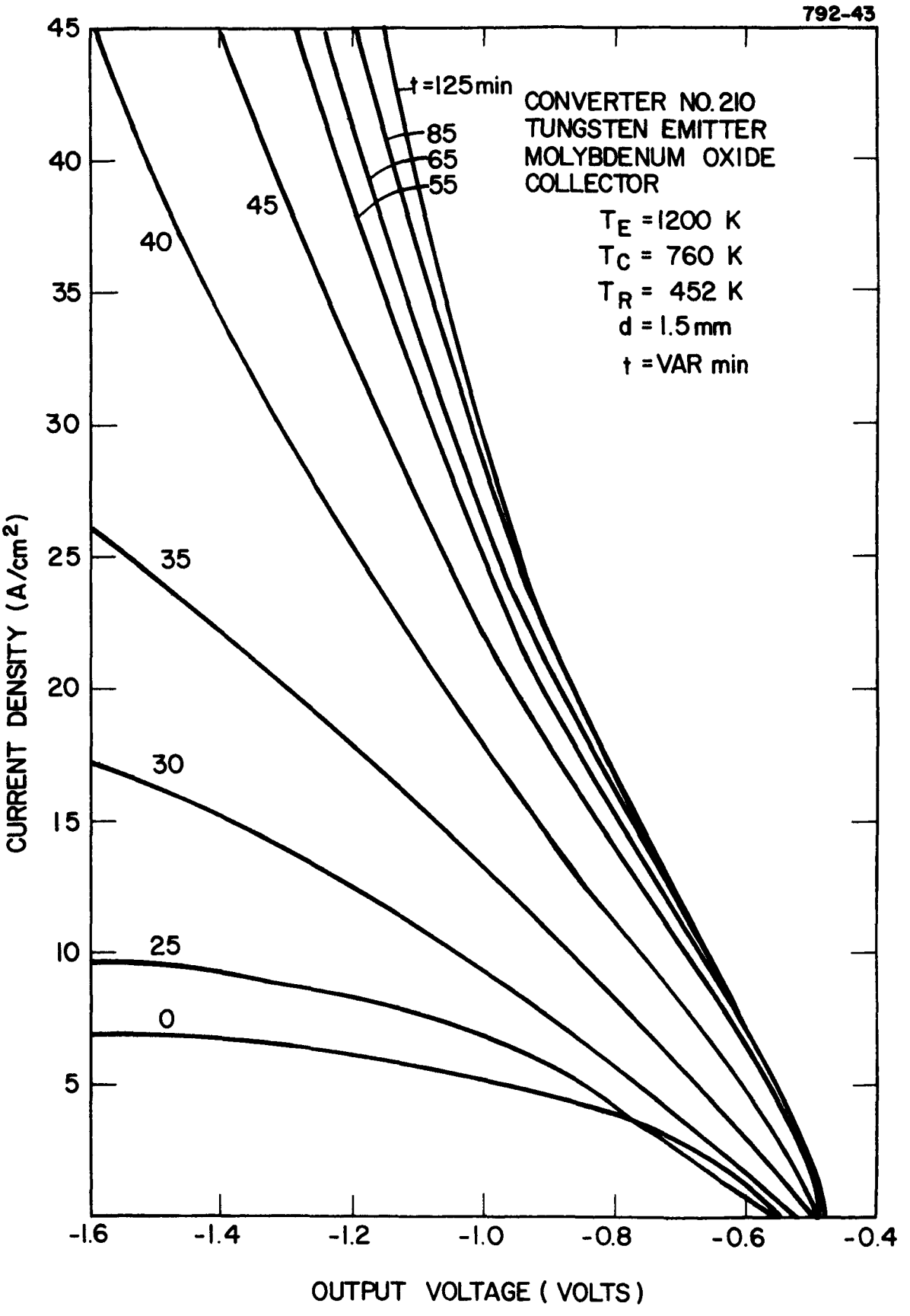

Figure 30. Time-Dependent Changes in Saturation Current

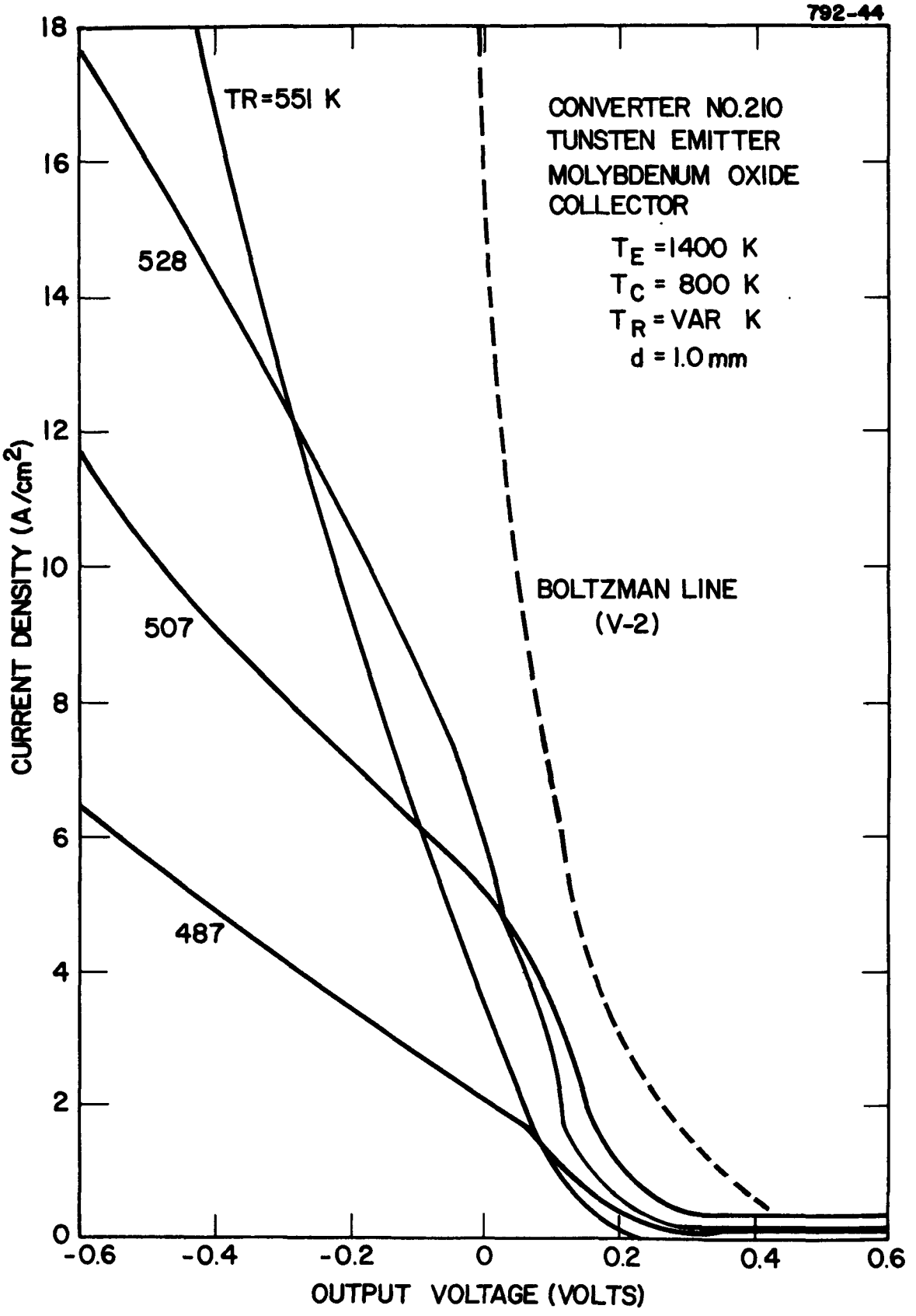

Figure 31. Cesium Family for Converter No. 210

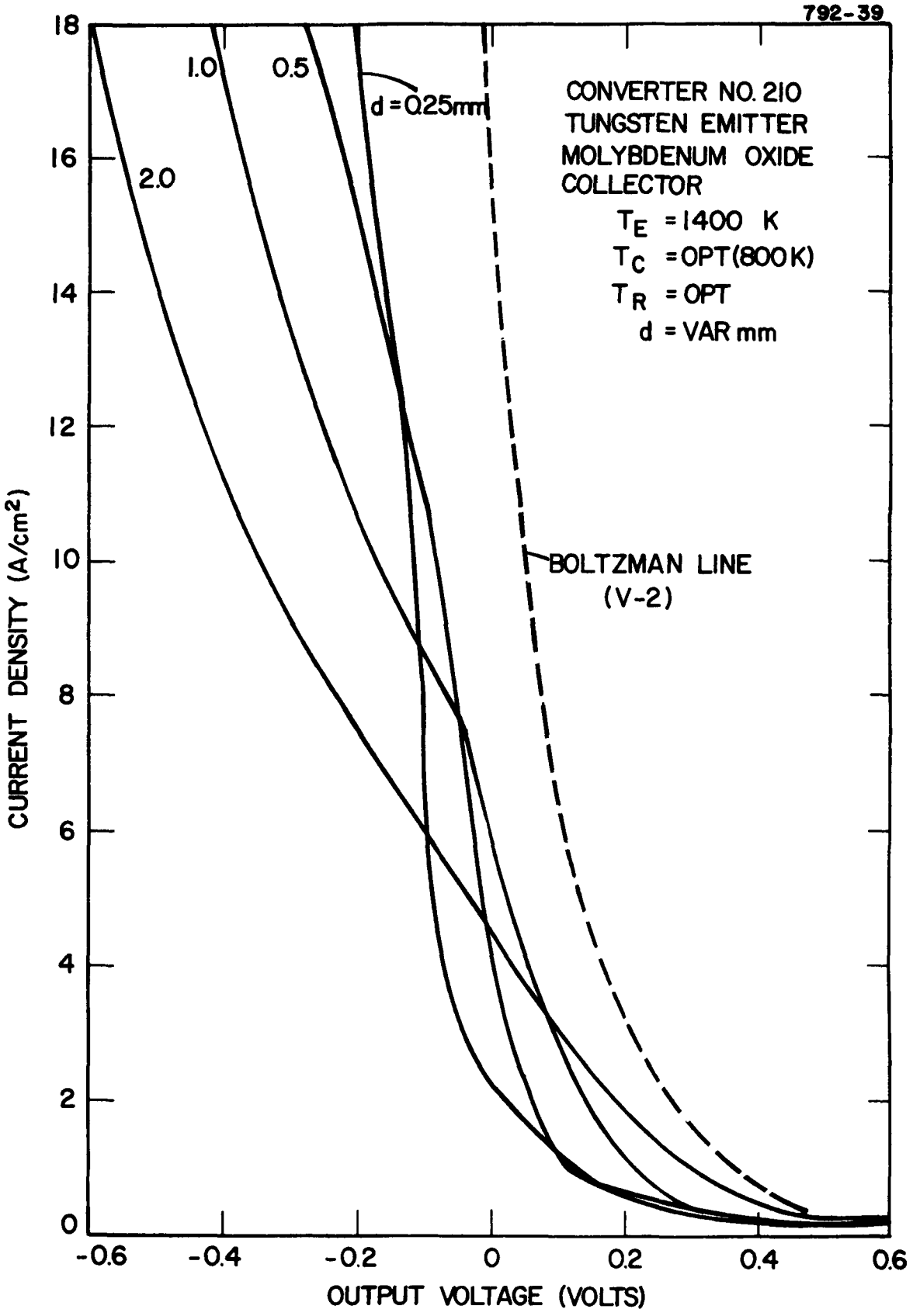

Figure 32. Optimized Converter Performance at Various Spacings, T_E = 1400 K

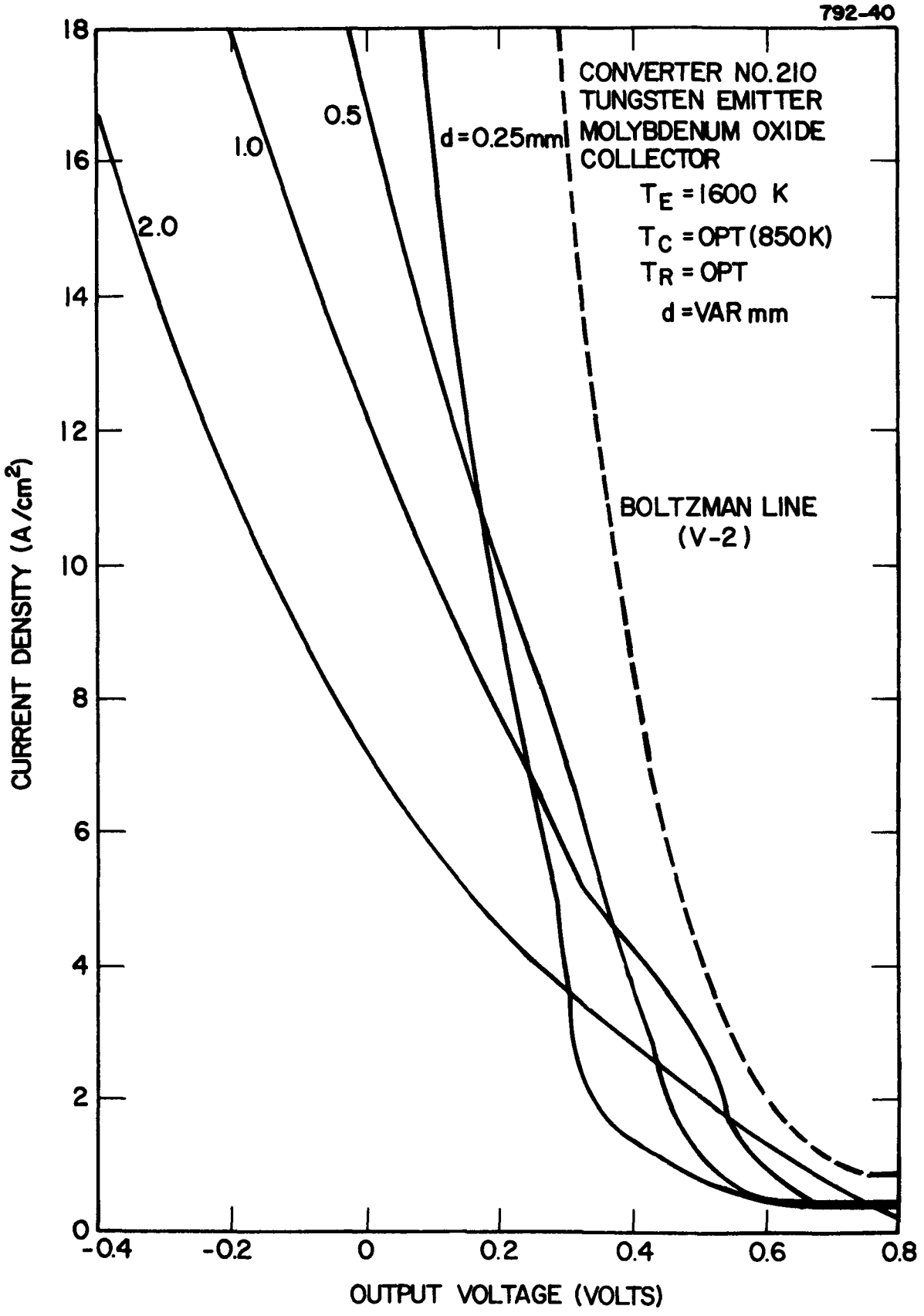

Figure 33. Optimized Converter Performance at Various Spacings, T_E = 1600 K

were 2.08 and 2.12 eV at emitter temperatures of 1400 and 1600 K, respectively.

B. LANTHANUM HEXABORIDE BONDING

Additional studies of bonding LaB_6 to emitter substrates have been carried out during this reporting period. The results are summarized in Table II. A promising approach has been the direct attachment of LaB_6 to the substrate using graphite powder. Although no metallurgical bond was observed, the temperature difference between the substrate and LaB_6 was considered low enough to be useful for constructing a converter for short-term testing.

The examination of LaB_6 bonding Sample No. 20 has been continued. A conductive gold coating was applied. X-ray spatial distribution maps were constructed that present the elemental distribution over selected areas of the sample. The area scanned can be related to the topographic phototgraph obtained by using the specimen current mode of presentation. The data for the two types of interfaces are as follows:

In Figure 34 the zone between the original molybdenum surface (which after the reaction was most likely a MoB phase) and the LaB_6 region shows the distribution of the two elements, molybdenum and lanthanum, as well as an overall scan for the presence of rhenium.

In Figure 35 the zone between the original rhenium foil and the LaB_6 region is shown in the specimen current photograph. These areas in the photograph related to the rhenium and lanthanum elemental distributions and the overall molybdenum distribution. No significant amounts of molybdenum are present in this region.

TABLE II

LaB_6 Bonding Tests

No.	Configuration	Bonding	Post Bond Treatment
28	LaB_6/Re 1" dia disc of Re	1270 C	Did not bond
28 A	LaB_6/Re 0.600 dia disc of Re	1460 C	Poor bond, $\Delta T \approx 250$ C
28 B	LaB_6/Re 0.600 dia disc of Re	1460 C	Poor bond, $\Delta T \approx 250$ C
29	LaB_6/C/W	1450 C	No bond
30	LaB_6/Ta same LaB_6 as No. 29	1296 C	Uniform temperature until unintentional power shut down, sample was loose
31	LaB_6/W same LaB_6 as No. 29	1289 C	No bond

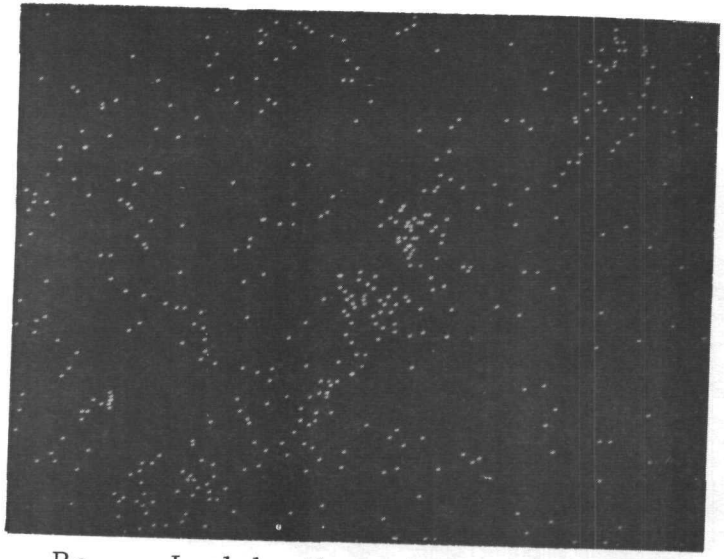

Re L alpha X-ray Map 400 X

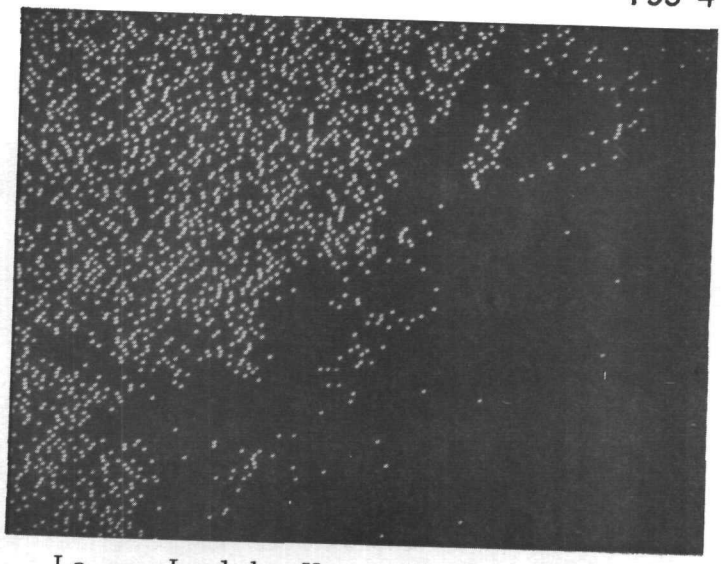

La L alpha X-ray Map 400 X

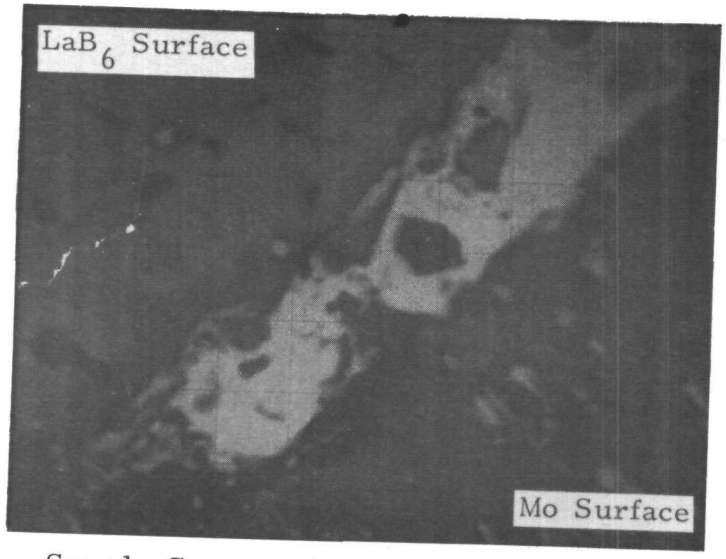

Sample Current (- mode) 400 X

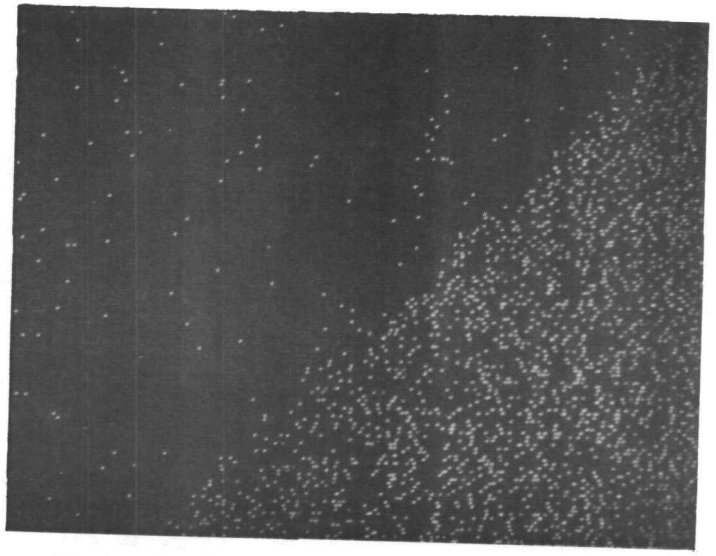

Mo L alpha X-ray Map 400 X

Figure 34. Lanthanum Hexaboride/Molybdenum Interface - Sample #20

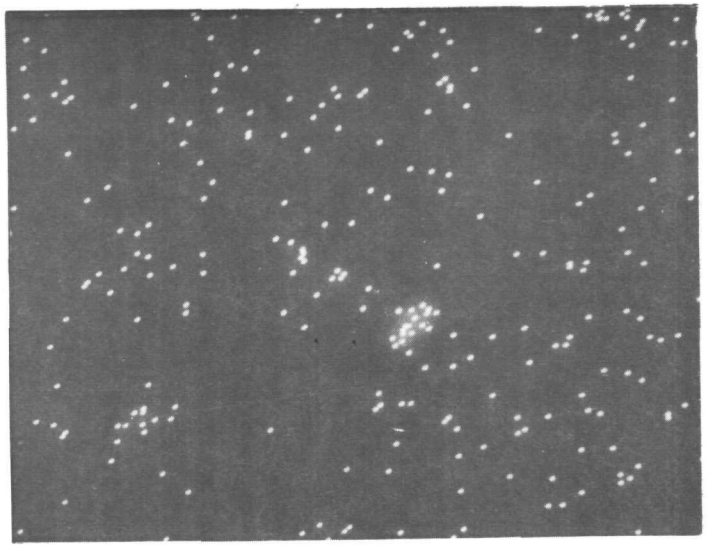

Mo L alpha X-ray Map 400 X

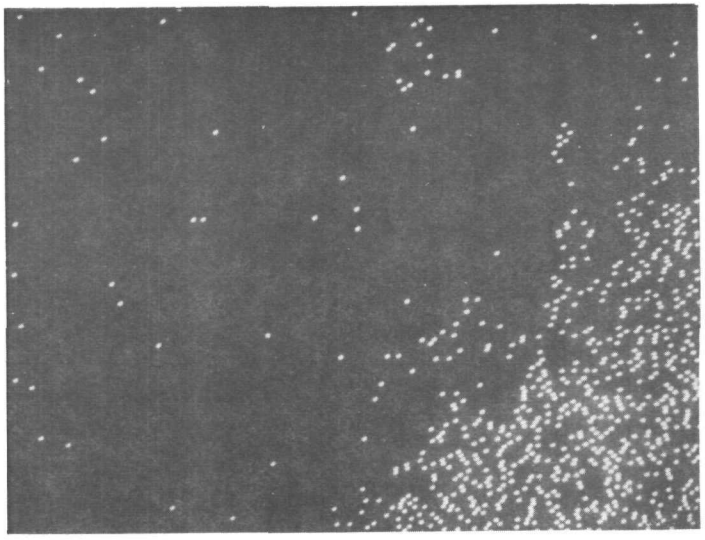

La L alpha X-ray Map 400 X

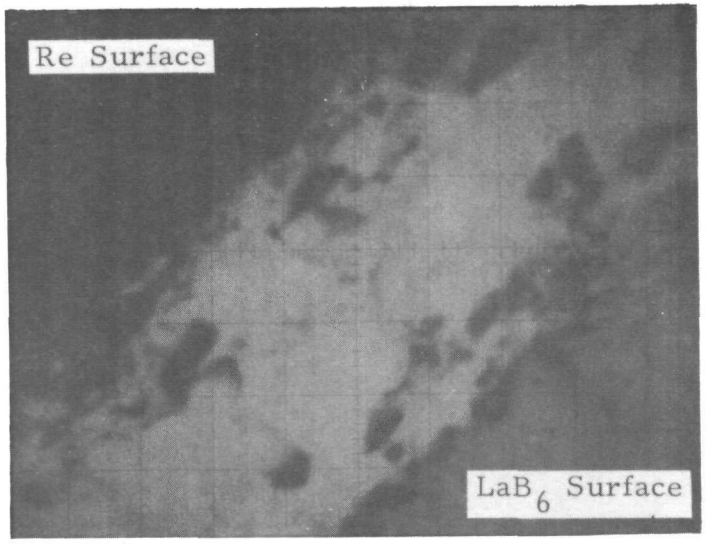

Sample Current (- Mode) 400 X

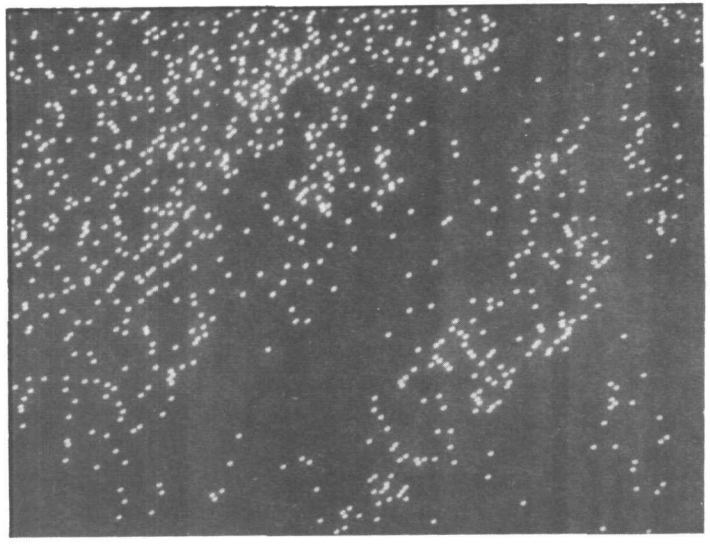

Re L alpha X-ray Map 400 X

Figure 35. Lanthanum Hexaboride/Rhenium Interface - Sample #20

In addition to the spatial distribution maps, various regions in the interfaces were scanned in order to determine what elements might be present. Such a scan along the interface is shown in Figure 34. The narrow white band in the sample current photograph shows that all three elements, molybdenum, lanthanum, and rhenium, are present. The spectrum does show gold, but this is the coated layer applied to keep the sample conductive. A similar scan along the interface shown in Figure 35 did not show any molybdenum; however, both lanthanum and rhenium were detected.

In order to obtain data on the distribution of the detected elements in the interface regions, a series of scans were taken across the interfaces. In this case, the x-ray detectors were tuned for the specific element and the sample traversed under the electron beam while the x-ray intensity was monitored on a strip chart recorder.

The surfaces of this composite sample were extremely non-uniform since some surfaces were pressed powders and others were two-phase regions. In the latter cases, the extreme differences in hardness usually resulted in some relief polishing so that the surfaces were rough or pitted. Although these surface features tended to mask the uniformity of the metallic distribution, some general features are noted. The lanthanum distribution in Figure 36 reflects the porosity of that phase. However, the data show that the lanthanum is confined almost exclusively in the LaB_6 zone of the sample. The distribution of the molybdenum is varied (most likely because of the presence of both metallic molybdenum, perhaps some oxides, and definitely a boride phase) in the region examined. However, there is very little, if any, diffusion of the molybdenum into the LaB_6 zone.

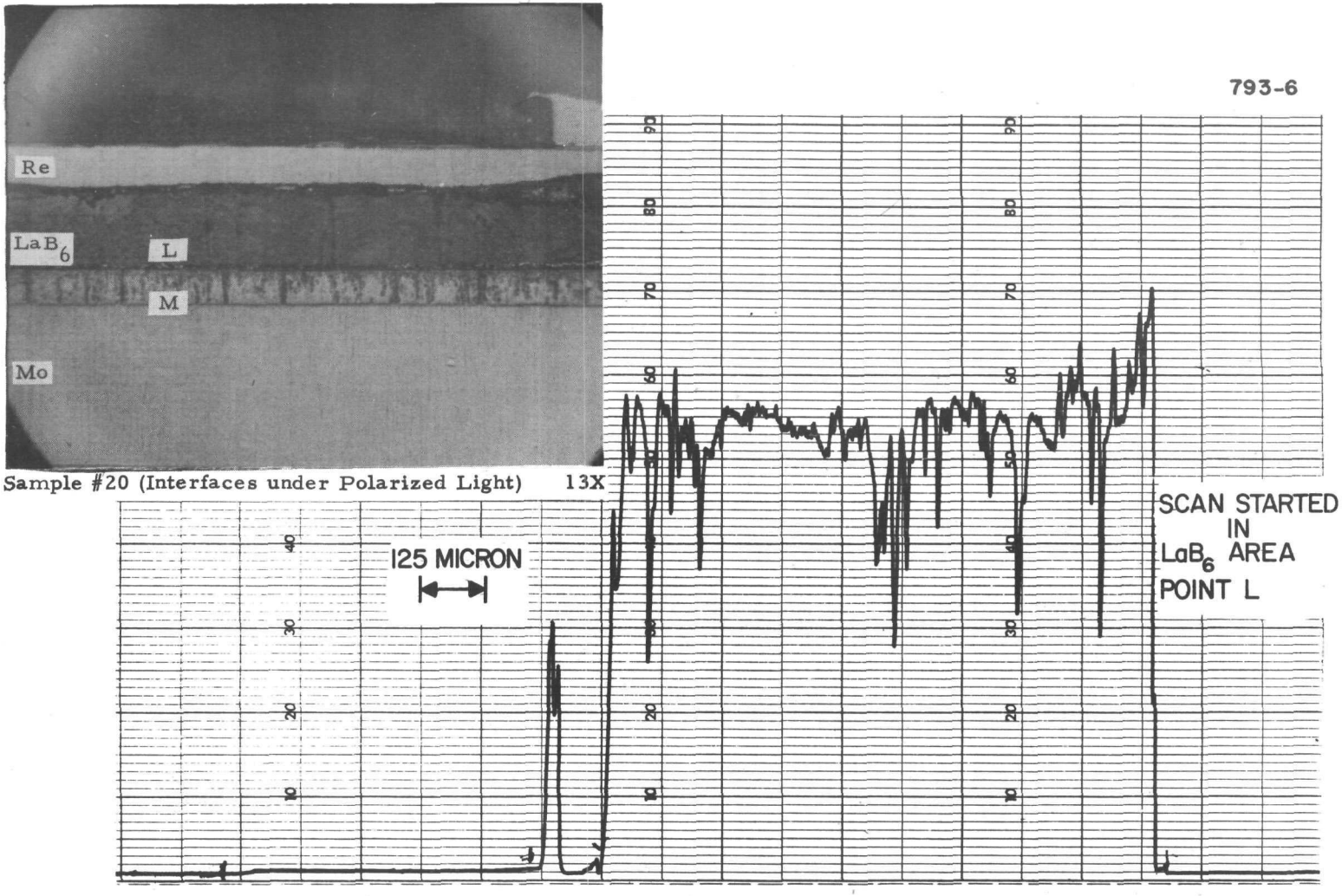

Figure 36. Distribution of La Across the Interface, as Noted, as Measured by the X-ray Intensity from La L alpha at 47.2°

The most unexpected observation was the distribution of rhenium across the interface. As expected, the x-ray intensities recorded while on the rhenium foil are rather uniform. The interface between the rhenium and the LaB_6 is rather abrupt and does not show any significant diffusion gradient across the interface. However, within the LaB_6 there are considerable regions of very high rhenium concentration. The distribution is that which one would expect from particles. In order to confirm this type of distribution, additional scans have been taken at different portions of the interface zone. In all cases, the same type of non-uniform rhenium distribution within the LaB_6 zone has been noted. The variation in the x-ray intensities of the rhenium areas in the LaB_6 zone and the intensities in the rhenium foil area suggest that the rhenium-containing regions in the LaB_6 zones may be a compound or another phase of rhenium (since the intensities are lower).

It is possible that the distribution of the rhenium in the LaB_6 region is due to a diffusion process. Since the LaB_6 material is a compressed powder, there is undoubetedly a larger percentage of voids and grain-boundaries within such a material. The non-uniform distribution of the rhenium in the LaB_6 may reflect the different rates of diffusion when the process is along or across grain boundaries. The width of the rhenium-rich regions can be measured from the scan rate data. These regions are about 50 to 60 microns in width along the scan direction. This range of dimensions could be of the same order as the dimensions of LaB_6 grains in the compacted LaB_6 pellet. Thus the rhenium metal may be interdiffused between the LaB_6 grains as well as diffused into an individual grain.

The data obtained from these examinations suggest that there is very little interdiffusion of the molybdenum into the LaB_6 or the LaB_6 into the molybdenum, except for some decomposition of the LaB_6 to provide a source of boron for the formation of molybdenum boride phases. There is, however, considerable evidence that the rhenium does diffuse into the LaB_6 regions and could possibly form compounds with the LaB_6.

Samples of $LaB_{6.5}$ bonded to standard variable-spacing converter-emitter substrates have been received from LASL. One of these is being prepared for installation into a variable-spacing converter. Another sample will be examined in the Surface Characterization Chamber.

V. POST OPERATIONAL DIAGNOSTICS

No post operational diagnostics were performed on JPL converters during this reporting period.

VI. VARIABLE-SPACING TEST STAND

Since this task is complete, no work was performed during this reporting period.

REFERENCES

1. C. C. Wang, "Topical Report: Numerical Solution of the Thermionic Diode Plasma Equation with the Electron Temperature as a Function of Position, " Thermo Electron Corp. Report No. TE4237-148-78, April 1978.

2. DOE/JPL Advanced Thermionic Technology Program, Progress Report No. 36, Thermo Electron Corp. Report No. TE4258/4247-89-79.

3. T. H. Pigford, "Chemical Equilibria in a Cs-O Diode with Tungsten Emitter and Molybdenum Collector" Report No. TE5114-58-70. For internal use only, NASA-Lewis and Thermo Electron Corp., Waltham, MA, 1970.

4. F. Fraim, F. Holly and L. Van Someren, "Molybdenum Trioxide as an Oxygen Source, " Final Report, Research in Thermionic Conversion, September 1966 to September 1967. Thermo Electron Corp., Waltham, MA.